J. Fluid Mech. (1995), *vol.* 293, *pp.* 237–268

Hysteresis in Faraday resonance

By S. P. DECENT AND A. D. D. CRAIK

School of Mathematical and Computational Sciences, University of St Andrews, St Andrews, Fife KY16 9SS, Scotland, UK

(Received 18 August 1994 and in revised form 19 January 1995)

Faraday waves arise on the surface of a liquid in a container that is undergoing vertical periodic oscillations. Hysteresis occurs when both finite-amplitude solutions and the flat-surface solution are available. We derive a nonlinear model of Faraday resonance, extending the Lagrangian method of Miles (1976). The model is used to investigate hysteresis. The theoretical results are compared to previous experimental studies and to some new observations. It is found necessary to retain damping and forcing terms up to third-order in wave amplitude, and also the fifth-order conservative frequency shift, in order to achieve agreement with experiments. The latter fifth-order term was omitted from all previous studies of Faraday waves. The lower hysteresis boundary in forcing-frequency space is found in most cases to be defined by the lower boundary above which non-trivial stationary points exist. However, the stability of stationary points and the existence of limit cycles are also found to be factors in determining the lower hysteresis boundary. Our results also suggest an indirect method for estimating the coefficient of cubic damping, which is difficult to obtain either experimentally or theoretically.

1. Introduction

Faraday resonance is responsible for the excitation of surface waves in a vertically oscillating container, the name deriving from a paper by Faraday (1831). Benjamin & Ursell (1954) showed that the linear problem is characterized by Mathieu's equation. Miles (1976, 1984, 1993) has studied nonlinear effects, adopting a variational approach. A good overview of the subject is given by Miles & Henderson (1990).

Hysteresis occurs when constant finite-amplitude solutions and the flat-surface solution are both available for a particular frequency and amplitude of sinusoidal forcing, with the observed behaviour being dependent upon the initial conditions. Both the linear stability boundary of the flat-surface solution and the lower hysteresis boundary depend on the frequency and the amplitude of the forcing. In the frequency-amplitude plane, the stability boundary has a hyperbolic shape with its minimum (in amplitude) at the resonant frequency equal to twice that of the natural water wave frequency. In this plane, the hysteresis region is the area between the two boundaries.

A mathematical model of Faraday resonance is derived here which captures the essential features of hysteresis that have been observed in some experiments (Simonelli & Gollub 1989; Douady 1990; Craik & Armitage 1995). Hysteresis has often been observed for values of forcing below the minimum value at which the flat-surface solution is unstable. The lower hysteresis boundary sometimes bifurcates from this neutral stability curve at a point away from the minimum and the hysteresis lower boundary is generally curved (figure 1 shows some new experimental observations of the linear stability boundary and the lower hysteresis boundary, for three neighbouring modes in a long rectangular tank; see Appendix A). The simple nonlinear theoretical

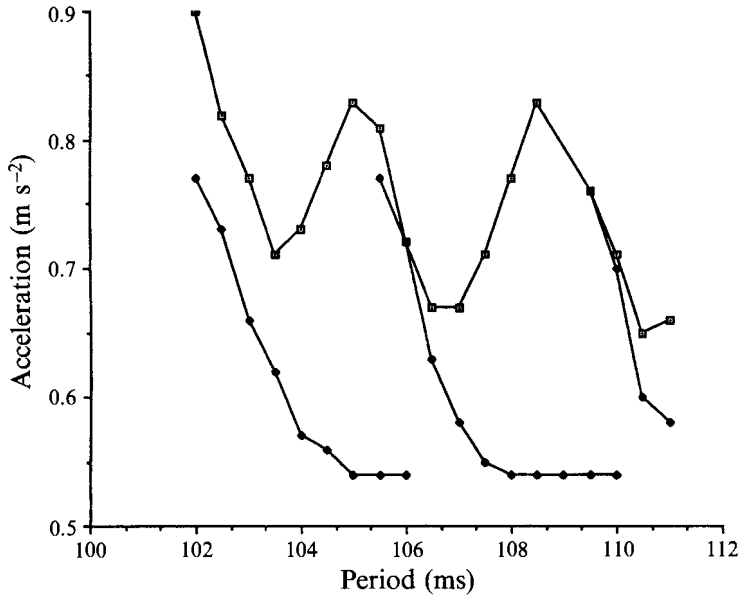

FIGURE 1. Experimental results showing acceleration (m s^{-2}) against period (ms) for three neighbouring modes of 21, 22 and 23 half-wavelengths in a rectangular tank of length 70 cm with a water depth of 1.3 cm.

model of a single mode by Miles (1976, 1984) has none of these features, in that it bifurcates from the minimum of the neutral stability curve, has no hysteresis below the minimum, and is a horizontal straight line (see figure 2(*a*) discussed below). Later models by Douady (1990) and Milner (1991) better describe the bifurcation of the hysteresis boundary from the linear stability boundary and allow hysteresis below the minimum; but the boundary remains straight and, if extended sufficiently, would meet the zero forcing axis (see figure 2(*b*) discussed below).

Craik & Armitage (1995) investigated theoretically and experimentally the hysteresis of two-dimensional Faraday waves in a long rectangular tank. Their theoretical model yields a variety of more realistic-looking hysteresis regions, though certain terms neglected (a fifth-order, in wave amplitude, conservative frequency shift, and one of the third-order forcing terms) in their model are likely to be of comparable size to those retained. Further, they did not calculate the coefficients of the terms in their equations for particular experimental configurations but considered instead the general form of the equations. Accordingly, they did not investigate the dependence of hysteresis upon depth, surface tension, wavelength, tank dimensions, etc.

The present paper, which follows on from Craik & Armitage (1995), calculates the various coefficients and provides a more rational derivation of the governing evolution equation which leads to the retention of the previously omitted fifth-order conservative frequency shift. We find that this fifth-order conservative term, a third-order forcing term, and a third-order damping term all combine to yield hysteresis regions similar to those observed in experiments.

The simplest nonlinear model of Faraday resonance is provided by the equation

$$\dot{A} = -\mu A + \mathrm{i}\Omega A + \mathrm{i}FA^* + \mathrm{i}\Pi |A|^2 A, \tag{1.1}$$

(see Miles 1976, 1984) where A is the slowly-varying complex wave amplitude; the overdot denotes a time-derivative, the real constants μ, Ω, F represent non-dimen-

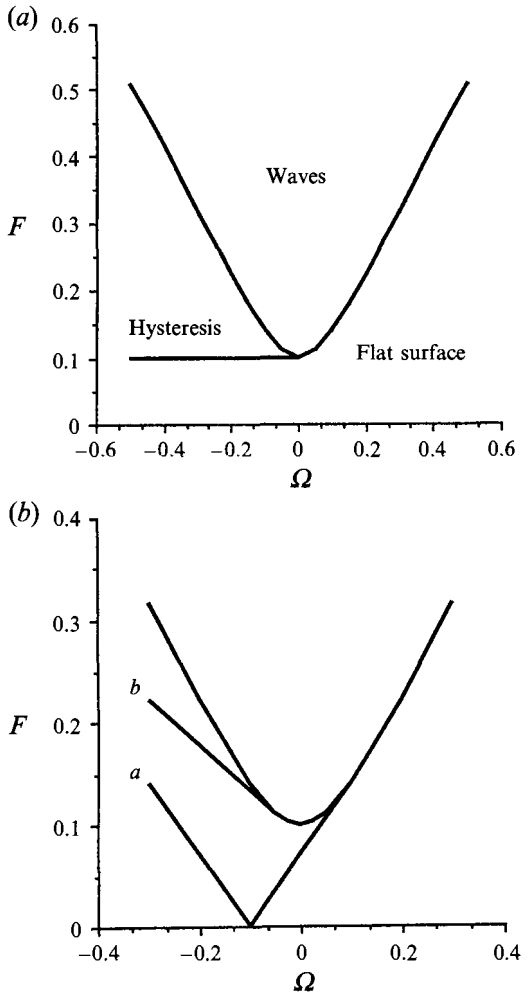

FIGURE 2. (*a*) Hysteresis diagram resulting from (1.1). (*b*) Hysteresis diagrams resulting from (1.2).

sionalized linear damping, frequency detuning from resonance, and the amplitude of the imposed vibrations, and Π represents the cubic coefficient of nonlinear (Stokes) frequency modification. Equilibrium solutions with $\dot{A} = 0$ give hysteresis as shown in figure 2(*a*), with the linear stability criterion $F \geqslant (\Omega^2 + \mu^2)^{1/2}$ and the lower hysteresis boundary $F = \mu$ on the left-hand side of the neutral stability boundary if Π is positive, and on the right-hand side if Π is negative.

Douady (1990) and Milner (1991) instead proposed

$$\dot{A} = -\mu A + \mathrm{i}\Omega A + \mathrm{i}FA^* + \mathrm{i}\Pi |A|^2 A + d|A|^2 A, \tag{1.2}$$

which retains a cubic correction to the damping with real coefficient d. However, they ignore cubic forcing and the firth-order conservative frequency shift that can be of the same order of magnitude (see later). This produces hysteresis diagrams of the form shown in figure 2(*b*) corresponding to d positive and negative, respectively. In the experiments by Simonelli & Gollub (1989) and Craik & Armitage (1995) hysteresis diagrams somewhat similar to figure 2(*b*) (line *a*) were found, but the lower hysteresis

boundary turned upwards before reaching the line $F = 0$ and was curved rather than straight. Douady (1990) interpreted his observations in terms of figure 2(*b*) (line *b*) (in fact, he observed no hysteresis in his experiment).

If $d < 0$, then the cubic correction to the damping in (1.2) acts to enhance dissipation; if it is positive then it will act in opposition to the linear damping term, reducing dissipation. In the latter case, so long as $d|A|^2$ is sufficiently small, the combined effect of the two terms is dissipative; however, if $d|A|^2$ exceeds μ then the model clearly breaks down. The coefficient d is difficult to calculate or to measure experimentally. Milner (1991) and Miles (1993) both give expressions for d that are based upon the assumptions of large depth and small wavelength and waveslope, and that the surface is uncontaminated. However, this is often not the case; in particular, in the experiments described here and in Craik & Armitage (1995) these assumptions do not hold. Even the linear damping coefficient μ is rather difficult to calculate or to measure experimentally. Both damping coefficients, μ and d, will depend upon viscous boundary layers at the sidewalls and the bottom of the tank, surface contamination, etc. (see Miles 1967). However, μ and d may be estimated indirectly by comparison of theory and experimental data, as described in §5.

Miles (1993) and Craik & Armitage (1995) both proposed a model equation that incorporates third-order forcing and third-order damping terms, namely

$$\dot{A} = -\mu A + \mathrm{i}\Omega A + \mathrm{i}FA^* + \mathrm{i}\Pi|A|^2A + d|A|^2A + \mathrm{i}\bar{F}(A^3 + 3|A|^2A^*), \tag{1.3}$$

and this produces hysteresis somewhat like those in figure 2(*b*) if $\bar{F}$ is chosen to be constant with respect to variations in F (note that an overbar does not denote complex conjugate). However, the coefficient of cubic-forcing $\bar{F}$ is proportional to F and so does not remain constant as F varies. Craik & Armitage (1995) showed that (1.3) can produce qualitatively all the observed effects of hysteresis. However, we here argue that a fifth-order conservative frequency shift may well be of comparable size to the cubic damping and cubic forcing terms, and so the inclusion of cubic damping and/or cubic forcing cannot be justified rationally without also retaining a fifth-order conservative term in $|A|^4A$. Here, as in Miles (1976, 1984), Umeki (1991) and Umeki & Kambe (1989), a rational theory is developed in terms of a small parameter ϵ which orders the terms in the governing equations. The cubic corrections to damping and forcing then appear formally at the same order in ϵ as an $|A|^4A$ conservative term.

Craik & Armitage (1995) mainly investigate a simplified version of (1.3) with the $\mathrm{i}\bar{F}A^3$ term neglected. This still produces hysteresis qualitatively similar to observations, while permitting precise analytic description. Miles (1993) mainly considered pattern selection and did not explicitly obtain the hysteresis boundary.

Retention of cubic damping without the fifth-order conservative term leads to unrealistic results when d is positive; for then (i) sufficiently large waves grow indefinitely, and (ii) unless d is very small then not all finite-amplitude states are stable foci as pointed out by Milner (1991) and Craik (1994).

Miles (1993) gives a formula for the coefficient of cubic forcing $\bar{F}$ in terms of depth, wavelength, surface tension and tank geometry, but the equivalent formula calculated here is not in agreement with this. In fact, Miles omitted the effect of the third harmonic of the dominant mode and we find that this contributes to the cubic forcing term. Our result and Miles' are often, but not always, close numerically.

The experimental work of Craik & Armitage (1995) investigated water depths of approximately 1 cm and 2 cm, for which the shape of hysteresis regions differed markedly. Here, in Appendix A, we describe results for the intermediate water depth of 1.3 cm, using the same apparatus. Figure 1 shows the hysteresis diagram for three

neighbouring modes in this experiment. These results resemble those of Craik & Armitage with a depth of 2 cm, but are unlike those at 1 cm. One reason for this is that the coefficient Π changes sign at a depth between 1 cm and 1.3 cm.

Our mathematical model is derived using the variational method due to Miles (1976, 1984, 1993), Umeki & Kambe (1989) and Umeki (1991). Along the way, the Lagrangian is calculated up to sixth-order in the generalized coordinate for any discrete set of wave modes in an arbitrary cylinder of cross-section S undergoing vertical oscillations; previously only fourth-order expansions have been derived (Miles 1976). The initial generality of this derivation potentially allows the fifth-order conservative terms to be incorporated into other (future) Faraday wave problems (e.g. mode competition and pattern selection). Here a single two-dimensional mode is considered, but this restriction is made only towards the end of §2. Examination of a different geometry or multiple wave interactions up to fifth-order could be done by using the general Lagrangian given in §2 as the starting point.

The derivation of the evolution equations is described in §3. This was algebraically very demanding and made extensive use of the symbolic manipulation computer package MAPLE. The nonlinear evolution equations are arrived at in the form

$$\left.\begin{aligned} \frac{\partial A}{\partial \tau_1} &= -\mu A + \mathrm{i}\Omega A + \mathrm{i}FA^* + \mathrm{i}\Pi |A|^2 A, \\ \frac{\partial A}{\partial \tau_2} &= N|A|^2 A + \mathrm{i}\bar{F}(A^3 + 3|A|^2 A^*) - \mathrm{i}h|A|^4 A, \end{aligned}\right\} \tag{1.4}$$

where τ_1 and τ_2 are separate slow and very slow timescales. The lower hysteresis boundary is investigated analytically in §4 and computationally in §5, by considering the existence of finite-amplitude stationary solutions. This allows a comparison between experimental and theoretical results. Numerical lower hysteresis boundaries from our model can be directly compared both to experimental observations and to the corresponding boundaries produced using the simpler model (1.3). This clearly shows that our model produces lower hysteresis boundaries that are quantitatively and qualitatively closer to observations than the previous 'best' model. Unfortunately, the experiment of Simonelli & Gollub (1989) cannot be described by our model since they observed three-dimensional waves and we have only considered two-dimensional waves here, though broad qualitative agreement is obtained. However, we anticipate that quantitative agreement can be achieved with a three-dimensional model similar to that of (1.4).

The numerical solutions also indirectly give estimates for the coefficient of cubic damping. This is achieved by choosing the coefficient so that the experimental and theoretical lower hysteresis boundaries are as close as possible (described later).

The stability of finite-amplitude solutions is investigated in §6. In some cases this leads to a revised theoretical prediction of the lower hysteresis boundary. Also time-dependent solutions of the evolution equation are briefly discussed. It is found that for the 2 cm depth experiment, the hysteresis region contains small stable limit cycles as well as stable stationary points: these limit cycles represent standing waves with amplitudes that experience a (small) slow oscillation on top of the fast sinusoidal oscillation at the basic frequency. This modulation of the wave amplitude would be difficult to observe experimentally with the present apparatus because the amplitude of the slow oscillation is never more than 10–20 % of the amplitude of the fast oscillation, and the latter amplitude is only a few millimetres. Further experimental work is needed with more accurate equipment to investigate these stable limit cycles.

Finally, a word on terminology. The *lower hysteresis boundary* is the theoretical lower boundary above which non-trivial solutions (stationary or time-oscillatory) exist and are stable. We will show that this usually coincides with the boundary above which non-trivial stationary points exist, since these stationary points are normally, but not invariably, stable. Sections 4 and 5 are concerned with calculating this boundary. However, as discussed in §6, the boundary above which non-trivial stationary points are stable is sometimes distinct from the boundary above which non-trivial stationary points exist, and in this case, the *lower stability boundary* is the appropriate lower hysteresis boundary.

2. Derivation of generalized Lagrangian

Consider capillary–gravity surface waves of an inviscid liquid of density ρ in a closed cylindrical container of cross-section S and depth d. Let (x, y, z) be the coordinates in a reference frame fixed in the container, with the bottom being identified as the plane $z = -d$, and S being independent of z. Let $\boldsymbol{n}$ be the outward normal to the fluid boundary, and let the free surface be denoted by $z = \eta(x, y, t)$. Assuming that the fluid motion is irrotational, it may be represented by the velocity potential $\phi(x, y, z, t)$ where $\boldsymbol{\nabla}\phi$ is the fluid velocity.

Following Miles (1976), the governing evolution equations can be derived using the Lagrangian method by applying the variational principle. The dynamic boundary condition is not explicitly used, but is instead incorporated intrinsically as part of the variational principle. The kinematical boundary-value problem is

$$\begin{gathered} \nabla^2\phi = 0, \quad (x, y) \in S, \; -d < z < \eta, \\ \boldsymbol{n}\cdot\boldsymbol{\nabla}\phi = 0 \text{ on container}, \quad \phi_z - \boldsymbol{\nabla}\eta\cdot\boldsymbol{\nabla}\phi = \eta_t \quad \text{on} \quad z = \eta. \end{gathered} \tag{2.1}$$

This can be derived from the variational problem

$$SI = \frac{1}{2}\iiint (\boldsymbol{\nabla}\phi)^2 \,\mathrm{d}S\,\mathrm{d}z - \iint (\phi)_{z=\eta}\,\eta_t \,\mathrm{d}S, \tag{2.2}$$

with respect to variations $\delta\phi$ of ϕ for given η.

Now take

$$\eta(x, y, t) = \eta_n(t)\,\psi_n(x, y), \quad \phi(x, y, z, t) = \phi_n(t)\,\chi_n(x, y, z), \tag{2.3a, b}$$

where η_n and ϕ_n are generalized coordinates, $\{k_n\}$ are the eigenvalues and $\{\psi_n\}$ and $\{\chi_n\}$ are the eigenfunctions from

$$(\nabla^2 + k_n^2)\,\psi_n = 0, \quad \boldsymbol{n}\cdot\boldsymbol{\nabla}\psi_n = 0 \quad \text{on} \quad \partial S, \tag{2.4a, b}$$

$$\iint \psi_m\,\psi_n \,\mathrm{d}S = \delta_{mn}\,S, \quad k_n = |\boldsymbol{k}_n|, \tag{2.4c, d}$$

$$\chi_n(x, y, z) = \psi_n(x, y)\,\mathrm{sech}\,(k_n d)\cosh\{k_n(z + d)\}, \quad n \text{ not summed}, \tag{2.4e}$$

and δ_{mn} is the Kronecker delta function.

Repeated indices are summed over the set of eigenfunctions except where stated.

Substituting (2.3) into (2.2) gives

$$I = \tfrac{1}{2} j_{mn}\,\phi_m\,\phi_n - d_{mn}\,\dot{\eta}_m\,\phi_n, \tag{2.5}$$

where

$$d_{mn} = S^{-1}\iint (\chi_n)_{z=\eta}\psi_m \,\mathrm{d}S, \quad j_{mn} = S^{-1}\iint \mathrm{d}S \int_{-d}^{\eta} \nabla\chi_m \cdot \nabla\chi_n \,\mathrm{d}z. \tag{2.6}$$

Applying the variational principle to (2.5) (by making I stationary with respect to variations in ϕ) gives

$$\phi_n = l_{nm}\dot{\eta}_m, \tag{2.7}$$

where

$$l_{nm} = d_{nl}j^{-1}_{lm}. \tag{2.8}$$

Substituting (2.3a) and (2.4e) into (2.6) and expanding about $z = 0$ using Taylor's theorem gives (see appendix of Miles 1976)

$$d_{mn} = \delta_{mn} + C_{lmn}j_n\eta_l + \tfrac{1}{2}C_{jlmn}k_n^2\eta_j\eta_l + \tfrac{1}{6}C_{ijlmn}j_n k_n^2\eta_i\eta_j\eta_l + \tfrac{1}{24}C_{hijlmn}k_n^4\eta_h\eta_i\eta_j\eta_l + \ldots, \tag{2.9}$$

$$\begin{aligned} j_{mn} = {} & \delta_{mn}j_m + (C_{lmn}j_m j_n + D_{lmn})\eta_l + \tfrac{1}{2}[C_{jlmn}(j_m k_n^2 + j_n k_m^2) + D_{jlmn}(j_m + j_n)]\eta_j\eta_l \\ & + \tfrac{1}{6}[C_{ijlmn}(j_m j_n k_m^2 + j_m j_n k_n^2 + 2k_m^2 k_n^2) + D_{ijlmn}(k_m^2 + k_n^2 + 2j_m j_n)]\eta_i\eta_j\eta_l \\ & + \tfrac{1}{24}[C_{hijlmn}(j_n k_m^4 + 3j_m k_n^2 k_m^2 + 3j_n k_n^2 k_m^2 + j_m k_n^4) \\ & + D_{hijlmn}(j_m k_m^2 + 3j_n k_m^2 + 3j_m k_n^2 + j_n k_n^2)]\eta_h\eta_i\eta_j\eta_l + \ldots, \end{aligned} \tag{2.10}$$

where

$$j_n = k_n \tanh(k_n d),$$

$$\left.\begin{aligned} C_{lmn} &= S^{-1}\iint \psi_l\psi_m\psi_n \,\mathrm{d}S, \quad C_{jlmn} = S^{-1}\iint \psi_j\psi_l\psi_m\psi_n \,\mathrm{d}S \quad \text{etc.} \\ D_{lmn} &= S^{-1}\iint \psi_l \nabla\psi_m\cdot\nabla\psi_n \,\mathrm{d}S, \quad D_{jlmn} = S^{-1}\iint \psi_j\psi_l\nabla\psi_m\cdot\nabla\psi_n \,\mathrm{d}S \quad \text{etc.} \end{aligned}\right\} \tag{2.11}$$

This now allows l_{mn} to be calculated explicitly up to the term in $\eta_h\eta_i\eta_j\eta_l$ from (2.8), though the result is very complicated and is not given here.

The dynamical problem is now considered by constructing the Lagrangian. The kinetic energy of the fluid is described by

$$T = \tfrac{1}{2}\rho\iiint (\nabla\phi)^2 \,\mathrm{d}S\,\mathrm{d}z = \tfrac{1}{2}\rho S j_{mn}\phi_m\phi_n = \tfrac{1}{2}\rho S a_{mn}\dot{\eta}_m\dot{\eta}_n, \tag{2.12}$$

where

$$a_{mn} = d_{mj}l_{jn}. \tag{2.13}$$

Substituting (2.9) and the expression for l_{mn} into (2.13) gives

$$a_{mn} = \delta_{mn}a_m + a_{lmn}\eta_l + \tfrac{1}{2}a_{jlmn}\eta_j\eta_l + \tfrac{1}{6}a_{ijlmn}\eta_i\eta_j\eta_l + \tfrac{1}{24}a_{hijlmn}\eta_h\eta_i\eta_j\eta_l + \ldots, \tag{2.14}$$

where

$$a_n = j_n^{-1}, \tag{2.15}$$

$$a_{lmn} = C_{lmn} - D_{lmn}a_m a_n, \tag{2.16}$$

$$a_{jlmn} = -D_{jlmn}(a_m + a_n) + 2D_{jmg}D_{lng}a_g a_m a_n, \tag{2.17}$$

$$\begin{aligned} a_{ijlmn} = {} & -2C_{ijlmn}k_n^2 k_m^2 a_m a_n - D_{ijlmn}\{(k_m^2 + k_n^2)a_m a_n + 2\} \\ & + 3D_{ijmg}D_{lgn}a_n(a_g + a_m) + 3D_{jlgn}D_{img}a_m(a_g + a_n) \\ & + 3C_{jlgn}D_{img}k_n^2 a_m a_n + 3C_{jlmg}D_{ign}k_m^2 a_m a_n \\ & - 6D_{lnf}D_{img}a_m a_n(a_g a_f D_{jgf} + C_{fjg}). \end{aligned} \tag{2.18}$$

The lengthy expression (2.19) for a_{hijlmn}, which is about six times longer than that for a_{ijlmn}, is not given here: a copy may be obtained from the authors or from the editor. In the above expressions and in (2.19) the summing convention may at first appear complicated, but is quite straightforward. For example in (2.18), i,j,l,m and n (which appear on the left-hand side) are not summed, while f and g (which do not) are summed over the set of participating modes.

In §3, where a single primary two-dimensional mode will be considered (along with its second and third harmonics), these considerably simplify using eigenfunctions and eigenvectors given by (3.13) and (3.14), respectively. The required non-trivial constants will then be

$$\left.\begin{aligned} &a_{112} = a_{121} = \frac{1}{\sqrt{2}}(1-2k_1^2 a_1 a_2), \quad a_{211} = \frac{1}{\sqrt{2}}(1+k_1^2 a_1^2),\\ &a_{123} = a_{132} = \frac{1}{\sqrt{2}}(1-6k_1^2 a_2 a_3), \quad a_{231} = a_{213} = \frac{1}{\sqrt{2}}(1-3k_1^2 a_1 a_3),\\ &a_{321} = a_{312} = \frac{1}{\sqrt{2}}(1+2k_1^2 a_1 a_2), \end{aligned}\right\} \tag{2.20}$$

$$\left.\begin{aligned} &a_{1111} = k_1^2 a_1(4k_1^2 a_1 a_2 - 1), \quad a_{1122} = 4k_1^2 a_2(k_1^2 a_1 a_2 - 2 + 9k_1^2 a_2 a_3),\\ &a_{2211} = k_1^2 a_1(k_1^2 a_1^2 - 2 + 9k_1^2 a_1 a_3), \quad a_{2112} = a_{1221} = 18k_1^4 a_1 a_2 a_3 - 2k_1^4 a_1^2 a_2,\\ &a_{1113} = a_{1131} = 12k_1^4 a_1 a_2 a_3 - \tfrac{3}{2}k_1^2(a_1 + a_3),\\ &a_{1311} = a_{3111} = k_1^2 a_1(1 - 4k_1^2 a_1 a_2), \end{aligned}\right\} \tag{2.21}$$

$$\left.\begin{aligned} &a_{11112} = a_{11121} = -\frac{1}{\sqrt{2}}k_1^2(4 - 49k_1^2 a_1 a_2 + 24k_1^4 a_1^2 a_2^2 - 27k_1^2 a_2 a_3 + 216k_1^4 a_1 a_2^2 a_3),\\ &a_{11211} = \sqrt{2}k_1^4 a_1(\tfrac{13}{4}a_1 + \tfrac{27}{4}a_3 + 6k_1^2 a_1^2 a_2 - 54k_1^2 a_1 a_2 a_3),\\ &a_{12111} = 4\sqrt{2}k_1^4 a_1^2, \end{aligned}\right\} \tag{2.22}$$

$$\left.\begin{aligned} &a_{21111} = \sqrt{2}k_1^4 a_1(-\tfrac{11}{4}a_1 + \tfrac{27}{4}a_3 + 6k_1^2 a_1^2 a_2 - 54k_1^2 a_1 a_2 a_3),\\ &a_{111111} = \tfrac{205}{2}k_1^4 a_1 - \tfrac{81}{2}k_1^4 a_3 - 9\frac{k_1^2}{a_2} - 200k_1^6 a_1^2 a_2 + 216k_1^6 a_1 a_2 a_3 + 96k_1^8 a_1^3 a_2^2 + 864k_1^8 a_1^2 a_2^2 a_3. \end{aligned}\right\} \tag{2.23}$$

The potential energy due to the free-surface displacement is

$$V_A = \rho \iint \mathrm{d}S \int_0^\eta (g + \ddot{z}_0)\, z\, \mathrm{d}z = \tfrac{1}{2}\rho S(g + \ddot{z}_0)\, \eta_n\, \eta_n, \tag{2.24}$$

where ρ is the density of the liquid, g is the acceleration due to gravity and $\ddot{z}_0$ is the vertical acceleration of the container. The potential energy due to the surface tension is given by

$$V_B = \gamma \iint ((1 + (\nabla\eta)^2)^{1/2} - 1)\, \mathrm{d}S, \tag{2.25}$$

where γ is the coefficient of surface tension.

This gives

$$V_B = \rho S c_{mn}\,\eta_m\,\eta_n, \tag{2.26}$$

where

$$c_{mn} = \frac{\gamma}{2\rho}(\delta_{mn}k_n^2 - \tfrac{1}{4}E_{jlmn}\,\eta_j\,\eta_l + \tfrac{1}{8}E_{hijlmn}\,\eta_h\,\eta_i\,\eta_j\,\eta_l - \ldots), \tag{2.27}$$

$$\left.\begin{aligned} E_{jlmn} &= S^{-1}\iint(\nabla\psi_j\cdot\nabla\psi_l)(\nabla\psi_m\cdot\nabla\psi_n)\,\mathrm{d}S,\\ E_{hijlmn} &= S^{-1}\iint(\nabla\psi_h\cdot\nabla\psi_i)(\nabla\psi_j\cdot\nabla\psi_l)(\nabla\psi_m\cdot\nabla\psi_n)\,\mathrm{d}S.\end{aligned}\right\} \tag{2.28}$$

The Lagrangian is given by

$$L = (\rho S)^{-1}(T - V_A - V_B). \tag{2.29}$$

By defining

$$\omega_n^2 \equiv gk_n\tanh(k_n d)(1+\lambda^2k_n^2), \tag{2.30}$$

where ω_n is just the natural (linearized) frequency of the nth normal mode, d is the depth and $\lambda = (\gamma/\rho g)^{1/2}$ is the capillary length, the Lagrangian can be rearranged into

$$\begin{aligned} L = {} & \tfrac{1}{2}a_n(\dot\eta_n^2 - \omega_n^2\,\eta_n^2) - \tfrac{1}{2}\ddot z_0\,\eta_n\,\eta_n + \tfrac{1}{2}a_{lmn}\,\eta_l\,\dot\eta_m\,\dot\eta_n + \tfrac{1}{4}a_{jlmn}\,\eta_j\,\eta_l\,\dot\eta_m\,\dot\eta_n\\ & + \tfrac{1}{12}a_{ijlmn}\,\eta_i\,\eta_j\,\eta_l\,\dot\eta_m\,\dot\eta_n + \tfrac{1}{48}a_{hijlmn}\,\eta_h\,\eta_i\,\eta_j\,\eta_l\,\dot\eta_m\,\dot\eta_n + \frac{\gamma}{8\rho}E_{jlmn}\,\eta_j\,\eta_l\,\eta_m\,\eta_n\\ & - \frac{\gamma}{16\rho}E_{hijlmn}\,\eta_h\,\eta_i\,\eta_j\,\eta_l\,\eta_m\,\eta_n + \ldots. \end{aligned} \tag{2.31}$$

The higher-order terms in a_{ijlmn}, a_{hijlmn}, and E_{hijlmn} were not retained in the previous work of Miles (1976, 1984, 1993), Umeki & Kambe (1989) and Umeki (1991). At lower orders, the formulations are in agreement.

3. Derivation of evolution equation

The evolution equation for a single principal two-dimensional mode (along with its associated harmonics) will now be found, where there are no internal resonances.

The container oscillates as

$$z_0 = \epsilon^2 f\cos 2\omega t \quad (\epsilon^2\omega^2|f| \ll g), \tag{3.1}$$

where $0 < \epsilon \ll 1$ is a small parameter.

It will be found useful to put

$$f = f_0 + \epsilon^2 f_1 + O(\epsilon^4), \tag{3.2}$$

where f_0 arises in the $O(\epsilon^4)$ equation and the perturbation f_1 from this value arises in the $O(\epsilon^6)$ equation.

The generalized coordinate of the nth mode is written as (with n not summed)

$$\begin{aligned} \eta_n(t) = {} & \delta_{1n}\,\epsilon a_n(p(\tau_1,\tau_2,\epsilon)\cos(\omega t) + q(\tau_1,\tau_2,\epsilon)\sin(\omega t))\\ & + \epsilon^2 a_n(A_n(\tau_1,\tau_2)\cos(2\omega t) + B_n(\tau_1,\tau_2)\sin(2\omega t) + C_n(\tau_1,\tau_2))\\ & + \epsilon^3 a_n(D_n(\tau_1,\tau_2)\cos(3\omega t) + E_n(\tau_1,\tau_2)\sin(3\omega t) + F_n(\tau_1,\tau_2)) + O(\epsilon^4), \end{aligned} \tag{3.3}$$

where the terms in p and q arise only for the principal resonant mode ($n = 1$), $\tau_1 \equiv \epsilon^2\omega t, \tau_2 \equiv \epsilon^4\omega t$ are dimensionless slow time variables, taken to be independent,

$$a_n = 1/k_n \tanh(k_n d) \quad \text{and} \quad \delta_{1n} = \begin{cases} 1, n = 1 \\ 0, n \neq 1. \end{cases}$$

Only $n = 1, 2$ and 3 need to be considered here. Later (see equation (4.1)) p and q will be expanded in a series in ϵ^2 to emphasize the multiple timescales present in the problem.

Substituting (3.1), (3.2) and (3.3) into (2.31), and averaging over a $2\pi/\omega$ interval of t, gives:

$$\begin{aligned}
\langle L\rangle = {} & a_1^3\omega^2\epsilon^4\left[\frac{1}{2}\left(\frac{\partial p}{\partial\tau_1}q - \frac{\partial q}{\partial\tau_1}p\right) + \frac{1}{4\epsilon^2}\left(1-\frac{\omega_1^2}{\omega^2}\right)(p^2+q^2) + \frac{f_0}{2\epsilon^2 a_1}(p^2-q^2)\right] \\
& + a_n^3\omega^2\epsilon^4\left[\left(1-\frac{\omega_n^2}{4\omega^2}\right)(A_n^2+B_n^2) - \frac{\omega_n^2}{2\omega^2}C_n^2\right] + \tfrac{1}{32}\omega^2\epsilon^4 a_1^4 a_{1111}(p^2+q^2)^2 \\
& + \tfrac{1}{2}\omega^2\epsilon^4 a_1^2 a_n\left[(a_{11n} - \tfrac{1}{4}a_{n11})\{A_n(p^2-q^2) + 2B_n pq\} + \tfrac{1}{2}a_{n11}(p^2+q^2)C_n\right] \\
& + \tfrac{1}{2}a_1^3\omega^2\epsilon^6\left[\frac{\partial p}{\partial\tau_2}q - \frac{\partial q}{\partial\tau_2}p + \frac{f_1}{\epsilon^2 a_1}(p^2-q^2)\right] + \frac{3\gamma}{64\rho}\epsilon^4 a_1^4 E_{1111}(p^2+q^2)^2 \\
& + \epsilon^6 X\left(\begin{array}{l} p, q, f_0, \omega, \{\omega_n, a_n\}_{n=1,2,3}, \{A_n, B_n, C_n\}_{n=1,2,3}, \{D_n, E_n, F_n\}_{n=1,2,3} \\ \{a_{lmn}, a_{jlmn}\}_{j,l,m,n=1,2,3}, a_{11112}, a_{11121}, a_{11211}, a_{12111}, a_{21111}, a_{111111} \\ \rho, \gamma, g, E_{1111}, E_{1113}, E_{1122}, E_{111111}, \dfrac{\partial p}{\partial\tau_1}, \dfrac{\partial q}{\partial\tau_1}, \dfrac{\partial p}{\partial\tau_2}, \dfrac{\partial q}{\partial\tau_2} \end{array}\right) \\
& + O(\epsilon^8), \qquad (3.4)
\end{aligned}$$

where repeated indices are summed over the set of participating modes and X is a highly complicated $O(1)$ expression that occupies many pages in MAPLE and which is omitted here for brevity. The ordering in (3.4) is based upon $(\omega^2-\omega_1^2)/2\omega^2 = O(\epsilon^2)$ which selects the single principal mode being considered from this point onwards. In (3.4) there is summing over $n = 1, 2, 3$. From Hamilton's principle, $\langle L\rangle$ must be stationary with respect to variations of $A_n, B_n, C_n, D_n, E_n, F_n$. At $O(\epsilon^4)$ the averaged Lagrangian is made stationary with respect to variations in A_n, B_n, C_n (e.g. by solving $\partial\langle L\rangle/\partial A_n = 0$ for A_n). This gives (with n not summed)

$$\left.\begin{aligned}
(A_n, B_n) &= -\frac{a_1^2}{4a_n^2}\left(1-\frac{\omega_n^2}{4\omega^2}\right)^{-1}(a_{11n} - \tfrac{1}{4}a_{n11})(p^2-q^2, 2pq) \\
C_n &= \frac{a_1^2\omega^2 a_{n11}}{4a_n^2\omega_n^2}(p^2+q^2).
\end{aligned}\right\} \qquad (3.5)$$

Equations (3.5) are then substituted into $\langle L\rangle$. At $O(\epsilon^4)\langle L\rangle$ can then be made stationary with respect to variations in p and q, which gives evolution equations in p and q for τ_1 variations. These are the same equations as derived by Miles (1976, 1984), namely

$$\frac{\partial A}{\partial\tau_1} = -\mu A + \mathrm{i}\Omega A + \mathrm{i}F_0 A^* + \mathrm{i}\Pi|A|^2 A, \qquad (3.6)$$

where $A = p+\mathrm{i}q$, and μ is the coefficient of linear damping (artificially introduced at this stage) on the timescale τ_1. Also,

$$\Pi = -\tfrac{1}{4}a_1^2k_1^2 + a_1^3a_2k_1^4 + \frac{a_1\omega_1^2}{8a_2\omega_2^2}\{1+a_1^2k_1^2\}^2 + \frac{9\lambda^2a_1gk_1^4}{16\omega_1^2} - \frac{a_1}{4a_2}\left(1-\frac{\omega_2^2}{4\omega_1^2}\right)^{-1}\{\tfrac{3}{4}-2a_1a_2k_1^2-\tfrac{1}{4}a_1^2k_1^2\}^2 \quad (3.7)$$

is the coefficient of the cubic (Stokes) frequency modification (in agreement with Miles 1984) and

$$\Omega = \frac{1}{\epsilon^2}\left(1-\frac{\omega_1^2}{\omega^2}\right), \quad F_0 = \frac{2f_0}{a_1}. \quad (3.8)$$

(Note that the introduction of the linear damping term in (3.6) can be explained by using an appropriate dissipation function: see Milner 1991; Miles 1993).

Trivial and non-trivial equilibrium solutions of this can be found, and their local stability analysed (see e.g. Nagata 1989). Hysteresis is found as shown in figure 2(*a*) for $\Pi > 0$. When $\Pi < 0$, the lower hysteresis boundary is to the right, not to the left, of the neutral stability curve. Clearly, no non-trivial equilibrium exists for

$$F_0 < \mu, \quad (3.9)$$

a result sometimes at odds with experimental evidence, as already mentioned.

The above equilibrium is found by putting

$$p+\mathrm{i}q = a\,\mathrm{e}^{\mathrm{i}\theta}, \quad (3.10)$$

which gives

$$\left.\begin{aligned} \cos 2\theta &= \frac{\pm(F_0^2-\mu^2)^{1/2}}{-F_0}, \quad \sin 2\theta = \frac{\mu}{F_0}, \\ a^2 &= \frac{-\Omega\pm(F_0^2-\mu^2)^{1/2}}{\Pi} \end{aligned}\right\} \quad (3.11)$$

for the non-trivial solution. In §4(*a*) we shall perturb about this equilibrium on the line in forcing-frequency parameter space given by

$$F_0 = \mu, \quad \omega \leqslant \omega_1. \quad (3.12)$$

That is, we shall take (3.11) and (3.12) as the basic solution about which perturbations will be made.

The three eigenfunctions that must be taken into account are

$$\psi_1 = \sqrt{2}\cos\frac{m\pi x}{l}, \quad \psi_2 = \sqrt{2}\cos\frac{2m\pi x}{l}, \quad \psi_3 = \sqrt{2}\cos\frac{3m\pi x}{l}, \quad (3.13)$$

corresponding to spatial eigenvalues (i.e. wavenumbers)

$$k_1 = \frac{m\pi}{l}, \quad k_2 = \frac{2m\pi}{l}, \quad k_3 = \frac{3m\pi}{l}, \quad (3.14)$$

where l is the length of the container. These correspond to the two-dimensional primary near-resonant mode with m half-wavelengths within the channel length and its second and third forced harmonics.

The averaged Lagrangian is now made stationary with respect to variations in D_n, E_n, F_n giving

$$D_1 = -\frac{2\omega^2 p f_0 + \frac{1}{4}\omega^2 a_{1111} a_1^2 p(p^2-3q^2)}{a_1(9\omega^2-\omega_1^2)} + \frac{\omega^4 a_1 p(p^2-3q^2)}{8a_2(4\omega^2-\omega_2^2)(9\omega^2-\omega_1^2)}[16a_{112}^2+8a_{112}a_{211}-3a_{211}^2] - \frac{\gamma E_{1111} a_1 p(p^2-3q^2)}{8\rho(9\omega^2-\omega_1^2)}, \tag{3.15}$$

$$D_2 = 0, \tag{3.16}$$

$$D_3 = \frac{a_1^3\omega^2 p(p^2-3q^2)}{16a_3^2(9\omega^2-\omega_3^2)}\{a_{3111}+a_{1311}-3a_{1131}-3a_{1113}\} - \frac{\omega^4 a_1^3 p(p^2-3q^2)}{8a_2 a_3^2(4\omega^2-\omega_2^2)(9\omega^2-\omega_3^2)}(4a_{112}-a_{211})(2a_{321}-6a_{123}-3a_{231}) - \frac{\gamma E_{1113} a_1^3 p(p^2-3q^2)}{8\rho a_3^2(9\omega^2-\omega_3^2)}, \tag{3.17}$$

$$E_1 = -\frac{2\omega^2 q f_0 + \frac{1}{4}\omega^2 a_{1111} a_1^2 q(3p^2-q^2)}{a_1(9\omega^2-\omega_1^2)} + \frac{\omega^4 a_1 q(3p^2-q^2)}{8a_2(4\omega^2-\omega_2^2)(9\omega^2-\omega_1^2)}[16a_{112}^2+8a_{112}a_{211}-3a_{211}^2] - \frac{\gamma E_{1111} a_1 q(3p^2-q^2)}{8\rho(9\omega^2-\omega_1^2)}, \tag{3.18}$$

$$E_2 = 0, \tag{3.19}$$

$$E_3 = \frac{a_1^3\omega^2 q(3p^2-q^2)}{16a_3^2(9\omega^2-\omega_3^2)}\{a_{3111}+a_{1311}-3a_{1131}-3a_{1113}\} - \frac{\omega^4 a_1^3 q(3p^2-q^2)}{8a_2 a_3^2(4\omega^2-\omega_2^2)(9\omega^2-\omega_3^2)}(4a_{112}-a_{211})(2a_{321}-6a_{123}-3a_{231}) - \frac{\gamma E_{1113} a_1^3 q(3p^2-q^2)}{8\rho a_3^2(9\omega^2-\omega_3^2)}, \tag{3.20}$$

$$F_1 = F_2 = F_3 = 0. \tag{3.21}$$

It should be noted that (3.15) and (3.18) have dependence upon the forcing. It is these terms in f_0 that result in differences between the coefficient of cubic forcing found here and that given by Miles (1993), who omitted third harmonics.

It is now possible to make $\langle L\rangle$ stationary with respect to variations in p and q at $O(\epsilon^6)$. This gives a second evolution equation

$$\frac{\partial A}{\partial \tau_2} \equiv \frac{\partial}{\partial \tau_2}(p+\mathrm{i}q) = \mathrm{i}\bar{F}_1 A^* - \tfrac{1}{8}\mathrm{i}\mu^2 A + NA|A|^2 + \mathrm{i}\tilde{F}_0(A^3+3|A|^2A^*) - \mathrm{i}hA|A|^4. \tag{3.22}$$

which must be made compatible with (3.6).

Here

$$\frac{\tilde{F}_0}{f_0} = -\frac{a_{1111}}{4} - \frac{3k_1^4\gamma}{16\rho\omega_1^2} + \frac{2\omega_1^2 a_{112}^2}{a_2(4\omega_1^2-\omega_2^2)} + \frac{a_{211}^2\omega_1^4}{a_2(4\omega_1^2-\omega_2^2)}\left(-\frac{3}{8\omega_1^2}+\frac{a_1}{a_2\omega_2^2}\right) + \frac{4a_{112}a_{211}\omega_1^4}{a_2(4\omega_1^2-\omega_2^2)}\left(\frac{2}{8\omega_1^2}-\frac{a_1}{a_2\omega_2^2}\right) \quad (3.23)$$

is the coefficient of cubic forcing, $\bar{F}_1 = 2f_1/a_1$ is a small correction to the linear forcing coefficient, h is the fifth-order conservative nonlinear frequency shift, and N is a coefficient of cubic damping (as in Miles 1993; Douady 1990; Milner 1991); this cubic damping term is introduced artificially, as it is absent from the Lagrangian formulation; however, the introduction of damping terms into the model could be done *a priori* by the inclusion of a dissipation function, as in Milner (1991) and Miles (1993). The form of the amplitude-dependence of the cubic forcing term is in agreement with Miles (1993), though the coefficient (3.23) differs from Miles' (1993) coefficient (B 3); this is because Miles only considered the first and second harmonics in his calculation, while we also considered the third harmonic. See Appendix C for a comparison between our cubic forcing and that of Miles.

The inclusion of the third harmonic also resulted in our retaining the $-\mathrm{i}A\mu^2/8$ term which Miles did not derive; this is a small correction to the linear frequency shift term. This term is numerically very small and can be neglected in (3.22) by including it instead in (3.6). This results in the linear frequency detuning coefficient being replaced by $\Omega-\epsilon^2\mu^2/8$ which is equivalent to a very small change in the origin.

The coefficient h, which derives from the expression X in (3.4), has been calculated using MAPLE for the general case but is too lengthy to be given here, as it occupies several pages of text. However, h simplifies in two limiting cases, namely zero surface tension and infinite depth. For zero surface tension we find that

$$h = \frac{3\kappa^2 R(\kappa)}{2048(\kappa^2-1)^7(2\kappa^2-1)(4\kappa^2-1)}, \quad (3.24)$$

where

$$\left.\begin{aligned} R(\kappa) &= 64-66\kappa^2-4687\kappa^4+33\,170\kappa^6-101\,256\kappa^8 \\ &\quad +162\,208\kappa^{10}-139\,584\kappa^{12}+61\,248\kappa^{14}-10\,368\kappa^{16}, \\ \kappa &= \cosh(k_1 d). \end{aligned}\right\} \quad (3.25)$$

For infinite depth we find that

$$h = \frac{9S(\varsigma)}{2048(1+4\varsigma)^2(-1+2\varsigma)^2(-1+3\varsigma)(1+\varsigma)^2}, \quad (3.26)$$

where

$$\left.\begin{aligned} S(\varsigma) &= 432+1360\varsigma-12\,663\varsigma^2-34\,495\varsigma^3 \\ &\quad +16\,144\varsigma^4-12\,444\varsigma^5-98\,272\varsigma^6-47\,808\varsigma^7, \\ \varsigma &= \frac{\gamma k_1^2}{\rho g}. \end{aligned}\right\} \quad (3.27)$$

In (3.26) the denominator is singular, as expected, at the second- and third-harmonic resonant frequencies $\varsigma = \frac{1}{2}$ and $\frac{1}{3}$ (where this theory will break down). Notice that as the depth tends towards infinity in (3.24), and as the surface tension tends towards zero in (3.26) then $h \to -243/128$.

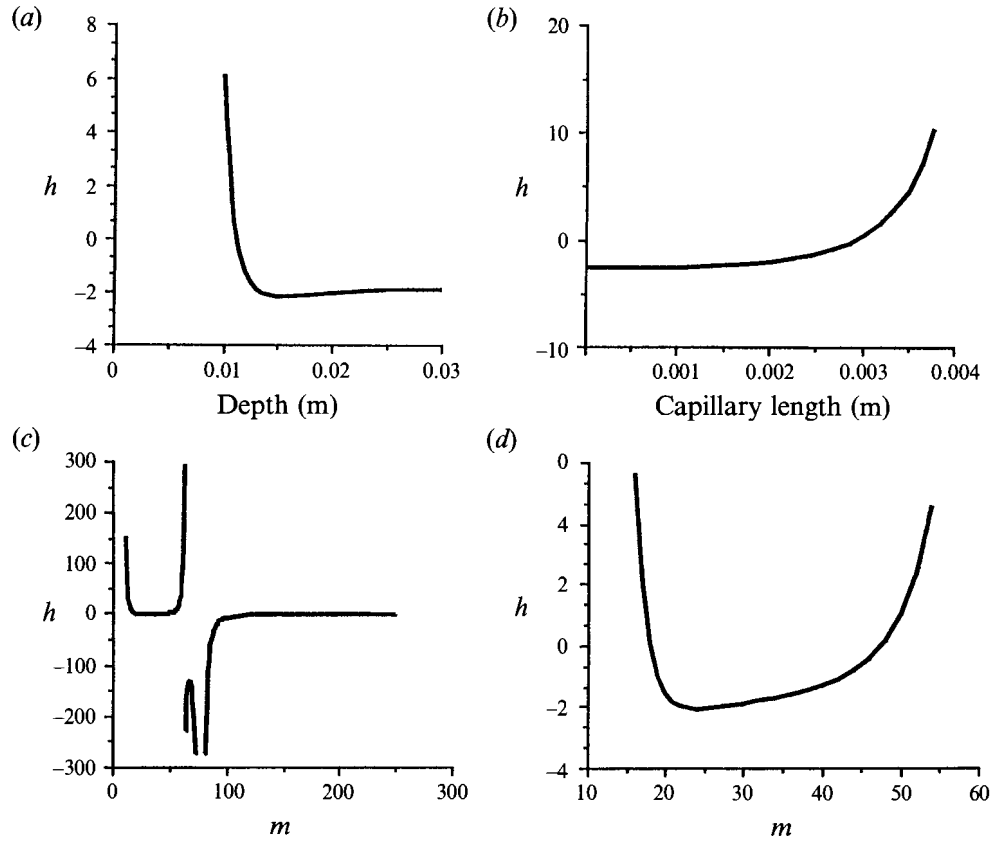

FIGURE 3. (*a*) h *vs.* depth for $m = 23$, $l = 0.7$, $\lambda = 0.002$. (*b*) h *vs.* capillary length for $m = 23$, $l = 0.7$, $d = 0.013\,52$. (*c*) h *vs.* m for $d = 0.013\,52$, $l = 0.7$, $\lambda = 0.002$. (*d*) Closer view of (*c*).

Figure 3 demonstrates how the full expression for h depends on depth, surface tension and the wavenumber parameter m as defined in (3.13) for a particular example. In figure 3(*c*), the missing parts of the graph correspond to second and third harmonic resonances where $|h|$ becomes very large and the ordering breaks down. Figure 3(*d*) shows a 'close-up' view of the part of figure 3(*c*) which is encountered in the experiments discussed in §5.

We now examine the compatibility of the two evolution equations (3.6) and (3.22), and so determine the region of hysteresis.

4. The lower hysteresis boundary

This section estimates the lower hysteresis boundary by analytically determining the curve above which finite-amplitude stationary solutions exist. The next section investigates this boundary computationally.

4.1. *Solution near* $F = \mu$

For steady solutions $(\partial A/\partial\tau_1) + \epsilon^2(\partial A/\partial\tau_2) = 0$, it is useful to apply the expansion

$$p + \mathrm{i}q = u + \mathrm{i}v + \epsilon^2(r + \mathrm{i}s) + O(\epsilon^4). \tag{4.1}$$

Combining (3.6), (3.22) and applying (4.1) gives at $O(1)$

$$-\mu C + \mathrm{i}\Omega C + \mathrm{i}F_0 C^* + \mathrm{i}\Pi|C|^2 C = 0, \quad \text{where} \quad C = u + \mathrm{i}v \tag{4.2}$$

which results in constant equilibrium values for u, v (which are just those of (3.10) and (3.11)). At $O(\epsilon^2)$, (3.6), (3.22) and (4.1) give

$$-\mu B+\Omega \mathrm{i}B+F_0\,\mathrm{i}B^*+\mathrm{i}\Pi\{2(ru+sv)\,C+|C|^2B\}$$
$$+\mathrm{i}\bar{F}_1\,C^*+\mathrm{i}\tilde{F}_0(C^3+3|C|^2C^*)+NC|C|^2-\mathrm{i}hC|C|^4=0, \quad (4.3)$$

where $B=r+\mathrm{i}s$ and C is given by (4.2).

At leading order, the lower boundary of the hysteresis region is given by (3.12), on which the amplitude C is

$$|C|^2=-\frac{\Omega}{\Pi}, \quad \text{phase}\,(C)=\tfrac{1}{4}\pi\,(\text{or}\,\tfrac{5}{4}\pi). \quad (4.4)$$

Substituting (4.4) into (4.3) and looking for equilibrium solutions gives rise to consistency conditions of the form

$$\begin{pmatrix} \Omega-\mu & \Omega+\mu \\ -\Omega+\mu & -\Omega-\mu \end{pmatrix}\begin{pmatrix} r \\ s \end{pmatrix}=\begin{pmatrix} c \\ d \end{pmatrix}, \quad (4.5)$$

where c and d are given by

$$c+\mathrm{i}d\equiv \mathrm{i}\bar{F}_1\,C^*+\mathrm{i}\tilde{F}_0(C^3+3|C|^2C^*)+NC|C|^2-\mathrm{i}hC|C|^4, \quad (4.6)$$

with $C=\pm(-\Omega/\Pi)^{1/2}\,\mathrm{e}^{\mathrm{i}\pi/4}$ from (4.4).

Clearly, for (4.5) to have a solution it is necessary that $c=-d$. This gives rise to

$$\tfrac{1}{2}\bar{F}_1\,a_1\equiv f_1=\frac{a_1\Omega}{2\Pi}(N+2\tilde{F}_0), \quad (4.7)$$

which is valid for $\omega\leqslant\omega_1$ (for $\Pi>0$). Notice that the h term does not contribute here because $ph(C)=\frac{1}{4}\pi, \frac{5}{4}\pi$; accordingly, this result is exactly the same as that obtained from (1.3). Equations (3.2), (3.8*b*), (3.12) and (4.7) together give the lower boundary of the hysteresis region as

$$F=\mu+\frac{\epsilon^2\Omega}{\Pi}(N+2\tilde{F}_0)+O(\epsilon^4). \quad (4.8)$$

This gives hysteresis below $F=\mu$ (for $\Omega<0$ when $\Pi>0$, and for $\Omega>0$ when $\Pi<0$) whenever $N+2\tilde{F}_0>0$, but it gives the lower hysteresis boundary above $F=\mu$ whenever $N+2\tilde{F}_0<0$.

It will be seen in §5 that our model gives better quantitative agreement with experimental observations than any previous theoretical model, the principal reason being that the fifth-order conservative term in (3.22) causes significant bending of the lower hysteresis boundary. Calculations extending (4.8) to next order in ϵ^2 (see Appendix D) give

$$F=\mu+\epsilon^2\frac{\Omega}{\Pi}(N+2\tilde{F}_0)+\epsilon^4\frac{\Omega^2}{4\mu\Pi^4}(8\tilde{F}_0\Pi^2(N+2\tilde{F}_0)+2h^2\Omega^2)+O(\epsilon^6). \quad (4.9)$$

Clearly, the fifth-order conservative term is responsible for bending the lower hysteresis boundary through the $h^2\Omega^4$ term. Although this calculation is only valid near to the line $F=\mu$, it supports the computational results of §5.

4.2. *Solution near minimum of neutral stability curve*

The lower hysteresis boundary has often been observed to bifurcate from the neutral stability curve at a point away from the minimum, and for there to be hysteresis beneath the minimum of the neutral stability curve at $\Omega=0$. Clearly (4.8) does not

model this behaviour, since the bifurcation from the neutral stability curve ($F^2 = \mu^2 + \Omega^2$) appears to occur at $\Omega = 0$, but the scalings break down when $\Omega \sim O(\epsilon^2)$. With a change of scalings, however, these features can be found in our evolution equations. We now rescale so that

$$\Omega = \epsilon\Omega_1, \quad \Pi = \epsilon\Pi_1, \quad F = \mu + \epsilon^2 F_1, \tag{4.10}$$

and replace (4.1) with

$$p + \mathrm{i}q = u + \mathrm{i}v + \epsilon(r + \mathrm{i}s) + \epsilon^2(U + \mathrm{i}V) + O(\epsilon^3). \tag{4.11}$$

These changes correspond to an analysis near to the minimum of the neutral stability curve. Note that (3.6) gives equilibrium solutions

$$|A|^2 = \frac{-\Omega \pm (F^2 - \mu^2)^{1/2}}{\Pi} = \frac{\epsilon(-\Omega_1 \pm (2\mu F_1)^{1/2})}{\Pi}, \tag{4.12}$$

so that the rescaling of Π ensures that A (and hence C) remains $O(1)$.

Applying the above scalings to our evolution equations and supposing that $\mathrm{d}A/\mathrm{d}t = 0$, gives

$$\left.\begin{aligned}
O(1): \quad & 0 = -\mu C + \mathrm{i}\mu C^*, \\
O(\epsilon): \quad & 0 = \mathrm{i}\Omega_1 C + \mathrm{i}\Pi_1 |C|^2 C - \mu B + \mathrm{i}\mu B^*, \\
O(\epsilon^2): \quad & 0 = N|C|^2 C + \mathrm{i}\tilde{F}_0(C^3 + 3|C|^2 C^*) - \mathrm{i}h|C|^4 C + \mathrm{i}F_1 C^* \\
& \quad -\mu D + \mathrm{i}\mu D^* + \mathrm{i}\Omega_1 B + \mathrm{i}\Pi_1 |C|^2 B \\
& \quad + 2\mathrm{i}\Pi_1 C(\mathrm{Re}\, B\, \mathrm{Re}\, C + \mathrm{Im}\, B\, \mathrm{Im}\, C),
\end{aligned}\right\} \tag{4.13}$$

where $C = u + \mathrm{i}v$, $B = r + \mathrm{i}s$, $D = U + \mathrm{i}V$.

At $O(1)$ we have that phase $(C) = \frac{1}{4}\pi, -\frac{3}{4}\pi$ as in (4.4), though the amplitude of C is left undetermined. At $O(\epsilon)$ we have

$$\mu(r - s) = -u(\Omega_1 + 2\Pi_1 u^2). \tag{4.14}$$

At $O(\epsilon^2)$ we have

$$\begin{pmatrix} -\mu & \mu \\ \mu & -\mu \end{pmatrix}\begin{pmatrix} U \\ V \end{pmatrix} = \begin{pmatrix} -2Nu^3 - 4\tilde{F}_0 u^3 - 4hu^5 + \Omega_1 s + 2\Pi_1 u^2(r + 2s) - F_1 u \\ -2Nu^3 - 4\tilde{F}_0 u^3 + 4hu^5 - \Omega_1 r - 2\Pi_1 u^2(2r + s) - F_1 u \end{pmatrix}. \tag{4.15}$$

The consistency condition on (4.15) along with (4.14) gives

$$u[4\Pi_1^2 u^4 + 4u^2(\Pi_1 \Omega_1 - \mu(N + 2\tilde{F}_0)) + \Omega_1^2 - 2F_1 \mu] = 0. \tag{4.16}$$

The non-trivial roots of (4.16) coalesce when

$$F_1 = \frac{(N + 2\tilde{F}_0)}{\Pi_1}\left(\Omega_1 - \frac{\mu(N + 2\tilde{F}_0)}{2\Pi_1}\right), \tag{4.17}$$

which is the lower hysteresis boundary. For (4.16) to have real non-trivial roots it is also necessary that

$$\left.\begin{aligned}
& \Omega_1 < \frac{\mu(N + 2\tilde{F}_0)}{\Pi_1} \quad \text{for} \quad \Pi_1 > 0, \\
\text{or} \quad & \Omega_1 > \frac{\mu(N + 2\tilde{F}_0)}{\Pi_1} \quad \text{for} \quad \Pi_1 < 0.
\end{aligned}\right\} \tag{4.18}$$

The equation for the neutral stability curve under these scalings is

$$F_1 = \frac{\Omega_1^2}{2\mu}. \tag{4.19}$$

Solving (4.17) with (4.19) gives the point of bifurcation of the lower hysteresis boundary from the neutral stability curve. This is

$$\Omega_1 = \frac{\mu(N+2\tilde{F}_0)}{\Pi_1}. \tag{4.20}$$

Equation (4.17) gives rise to a lower hysteresis boundary similar to (4.8), but shifted slightly; this correctly gives rise to a tangential bifurcation from the neutral stability curve, whereas (4.8) incorrectly meets the neutral curve at an angle at $\Omega_1 = 0$. This bifurcation point agrees with the corresponding result of Craik & Armitage (1995).

4.3. *Solutions close to neutral curve for* $\Omega \sim O(1)$

We now assume that $\Pi = \epsilon^2 \hat{\Pi}$ where $\hat{\Pi}$ is $O(1)$.

Applying the above rescaling and (4.1) to our stationary evolution equation gives

$$\left.\begin{aligned} O(1): \quad & -\mu C + \mathrm{i}\Omega C + \mathrm{i}F_0 C^* = 0, \\ O(\epsilon^2): \quad & -\mu B + \mathrm{i}\Omega B + \mathrm{i}F_0 B^* + \mathrm{i}\hat{\Pi}|C|^2 C + \mathrm{i}F_1 C^* \\ & + N|C|^2 C + \mathrm{i}F_0 \Gamma(C^3 + 3|C|^2 C^*) - \mathrm{i}h|C|^4 C = 0, \end{aligned}\right\} \tag{4.21}$$

where $C = u + \mathrm{i}v, B = r + \mathrm{i}s$. Note that the coefficient of cubic forcing is now taken to be $F\Gamma = F_0\Gamma + O(\epsilon^2)$, in line with Craik & Armitage (1995).

From the $O(1)$ equations we have

$$\left.\begin{aligned} F_0 &= (\mu^2 + \Omega^2)^{1/2}, \\ \text{phase}(C) &= \theta \quad \text{where } \mathrm{e}^{-2\mathrm{i}\theta} = \frac{\mu - \mathrm{i}\Omega}{\mathrm{i}F_0}. \end{aligned}\right\} \tag{4.22}$$

The $O(\epsilon^2)$ equations give

$$\begin{pmatrix} -\mu & -\Omega + F_0 \\ \Omega + F_0 & -\mu \end{pmatrix} \begin{pmatrix} r \\ s \end{pmatrix} = \begin{pmatrix} \mathrm{Re}\, Q \\ \mathrm{Im}\, Q \end{pmatrix}, \tag{4.23}$$

where

$$Q = -[\mathrm{i}\hat{\Pi}|C|^2 C + \mathrm{i}F_1 C^* + N|C|^2 C + \mathrm{i}F_0 \Gamma(C^3 + 3|C|^2 C^*) - \mathrm{i}h|C|^4 C] \tag{4.24}$$

and $\mathrm{ph}(C)$ is known from (4.22).

As the determinant of (4.23) is zero, we need

$$(\Omega + F_0)\,\mathrm{Re}\, Q + \mu\,\mathrm{Im}\, Q = 0, \tag{4.25}$$

which is equivalent to

$$\mathrm{Re}[(1 - \mathrm{e}^{2\mathrm{i}\theta}) Q] = 0, \tag{4.26}$$

using (4.22).

This gives the trivial solution and also a quadratic equation in $|C|^2$ which has roots

$$\left.\begin{aligned} |C|^2 &= \frac{\Lambda \pm (\Lambda^2 - 4h\Omega F_1(\mu^2 + \Omega^2)^{1/2})^{1/2}}{2h\Omega}, \\ \text{where} \qquad \Lambda &= \Omega\hat{\Pi} - \mu N - 2\Gamma(2\Omega^2 + \mu^2). \end{aligned}\right\} \tag{4.27}$$

The roots of (4.27) coalesce at the lower hysteresis boundary, where

$$F_1 = \frac{(\Omega\hat{\Pi} - \mu N - 2\Gamma(2\Omega^2 + \mu^2))^2}{4h\Omega(\mu^2 + \Omega^2)^{1/2}}. \tag{4.28}$$

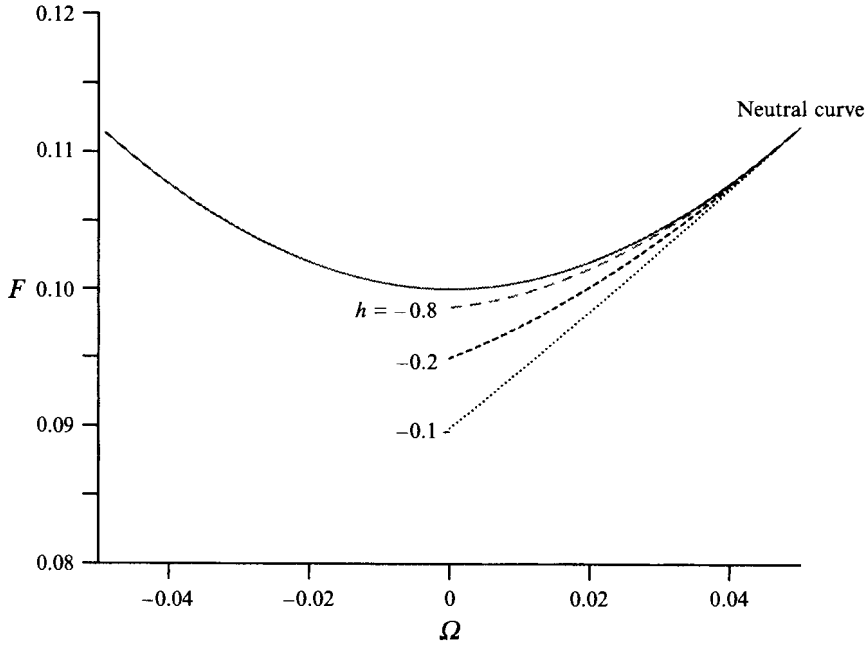

FIGURE 4. Lower hysteresis boundaries predicted by (4.31). Parameters $\mu = 0.1$, $\Gamma = 1.1$, $\epsilon^2 = 0.047$, $\Omega_{bif} = 0.05$, $h = -0.1, -0.2, -0.8$.

It should be noted that for hysteresis it is necessary that $F_1 < 0$ which implies that $h\Omega < 0$.

It is also necessary that the right-hand side of (4.27) must be positive. If $h\Omega < 0$ then it is necessary that $\Omega < \Omega_-$ or $\Omega > \Omega_+$ where

$$\Omega_\pm \equiv \frac{\hat{\Pi} \pm (\hat{\Pi}^2 - 16\Gamma\mu(N + 2\mu\Gamma))^{1/2}}{8\Gamma}, \tag{4.29}$$

assuming $\Gamma > 0$ (which is generally true – see Appendix C). Solving (4.28) together with the expression for the neutral curve shows that both Ω_- and Ω_+ correspond to bifurcation points. Substituting $\hat{\Pi} = \Pi/\epsilon^2$ into these bifurcation points and expanding in a Taylor series gives

$$\Omega_- = \frac{\epsilon^2\mu}{\Pi}(N + 2\mu\Gamma) = \frac{\epsilon^2\mu}{\Pi}(N + 2\tilde{F}_0), \tag{4.30}$$

which is identical to (4.20), and $\Omega_+ = O(1/\epsilon^2)$ which is probably spurious.

The behaviour of the lower hysteresis boundary near to the bifurcation point can be examined by putting $\Omega = \Omega_{bif} + \Delta$ in (4.28), where Ω_{bif} is the frequency offset corresponding to the bifurcation, and $|\Delta| \ll |\Omega_{bif}|$. Then

$$F_1 = \frac{\Delta^2(\hat{\Pi} - 8\Gamma\Omega_{bif})^2}{4h\Omega_{bif}(\mu^2 + \Omega_{bif}^2)^{1/2}} + O(\Delta^3). \tag{4.31}$$

Therefore as $|h|$ decreases, the lower hysteresis boundary will move more quickly away from the neutral curve. This result seems paradoxical; but since the scaling requires h to be $O(1)$, no singularity is expected as $|h| \to 0$.

Equation (4.31) is significant because it shows the fifth-order conservative term appearing in an expression for the lower hysteresis boundary at the lowest possible order, and this expression describes the lower hysteresis boundary at a point that is near to the neutral curve. So the fifth-order conservative term is playing an important role even close to the bifurcation point. It will be seen in the next section that the fifth-order conservative term also has large effects on the lower hysteresis boundary far from the neutral stability curve.

Figure 4 shows possible hysteresis diagrams produced from (4.31) near to the bifurcation point. It can be seen that increasing $|h|$ again causes an increase in the upwards curvature of the lower hysteresis boundary, though not for the same reason as in (4.9). Note that $|h| \ll 1$ would give downwards bending, but sufficiently small h values are ruled out by scaling assumptions. (Though (4.27) has simple poles at both $\Omega = 0$ and $h = 0$, this subsection has assumed that Ω and h are $O(1)$.)

5. Numerical work

Equations (3.6) and (3.22) give the composite equation

$$\begin{aligned}\frac{\mathrm{d}A}{\mathrm{d}t} &= \epsilon^2\omega\left(\frac{\partial A}{\partial \tau_1}+\epsilon^2\frac{\partial A}{\partial \tau_2}\right)\\ &= \epsilon^2\omega(-\mu A+\mathrm{i}\Omega A+\mathrm{i}FA^*+\mathrm{i}\Pi|A|^2A)\\ &\quad+\epsilon^4\omega(N|A|^2A+\mathrm{i}\tilde{F}(A^3+3|A|^2A^*)-\mathrm{i}h|A|^4A)=0,\end{aligned} \tag{5.1}$$

where the forcing expansion (3.2) has not been applied, and the small shift in the origin caused by the linear frequency detuning term in (3.22) has been ignored. Equation (5.1) has been examined computationally using a FORTRAN NAG routine. The model equation (1.3), previously discussed by Craik & Armitage (1995), which omits the h-term, has also been investigated numerically.

In order to compare theory with experiments, it is necessary to determine the scaling parameter ϵ^2 and to estimate N. Using (3.1), the r.m.s. acceleration is given by

$$\left(\frac{\omega}{2\pi}\int_0^{2\pi/\omega}(4\omega^2\epsilon^2 f)^2\cos^2 2\omega t\,\mathrm{d}t\right)^{1/2} = 2\sqrt{2}\omega^2\epsilon^2 f. \tag{5.2}$$

At the minimum of the neutral stability curve $F \equiv 2f/a_1 = \mu$. Therefore

$$\epsilon^2\mu \approx \frac{\alpha}{\sqrt{2}a_1\omega_1^2}, \tag{5.3}$$

where α is the experimentally observed r.m.s. acceleration at the minimum of the neutral stability curve. Without loss of generality, we choose $\mu = 1$, so that (5.3) gives ϵ^2. For the experimental observations shown in figure 1, this gives $\epsilon^2 = 0.047$ for the 22 half-wavelength mode. (The choice of $\mu = 1$ is equivalent to expanding the evolution equation in terms of a linear dissipation parameter $\epsilon^2\mu$.)

Equations (5.1) and (1.3) were each solved numerically by searching for the value of the forcing F that corresponds to the disappearance of finite-amplitude equilibrium solutions, for various chosen frequencies Ω. A comparison of the hysteresis diagrams resulting from three different models is shown in figure 5. There are two possible choices for the coefficient of cubic forcing, namely

$$\text{(i) } \tilde{F}_1 = f\Gamma \quad \text{or} \quad \text{(ii) } \tilde{F}_2 = f_0\Gamma, \tag{5.4}$$

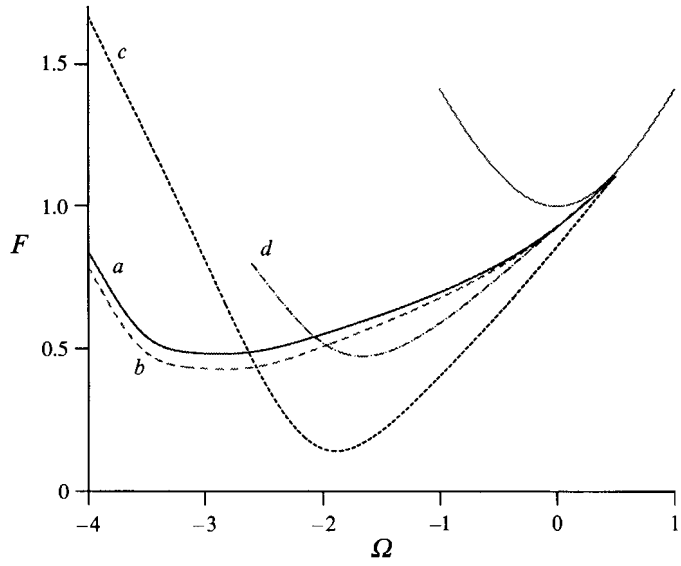

FIGURE 5. Existence of finite-amplitude fixed points for four different models: (*a*) our model (5.1) with $\tilde{F}_1$, (*b*) our model (5.1) with $\tilde{F}_2$, and (*c*) equation (1.3) with $\tilde{F}_1$ and (*d*) equation (1.3) with $\tilde{F}_1$ for $N = 1.57$. Parameters are $m = 22$, $l = 0.7$, $d = 0.013\,52$, $\lambda = 0.02$, $\mu = 1$, $N = 2.43$ except in (*d*), $\epsilon^2 = 0.047$, $h = -2.1$, $\Pi = 0.25$, $\Gamma = 1.1$.

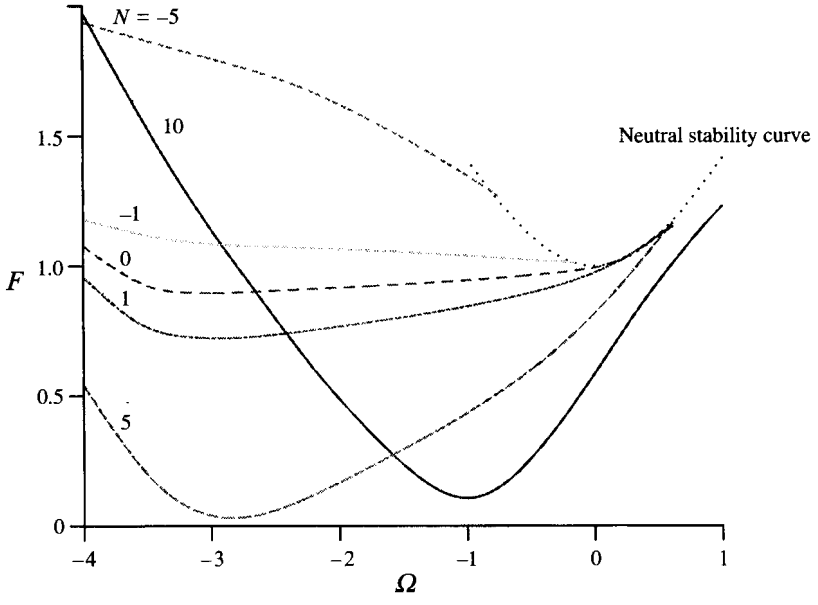

FIGURE 6. Existence of finite- amplitude fixed points for six different values of N. Other parameters as in figure 5.

where Γ is the expression in square brackets in (3.23). Cubic forcing coefficient $\tilde{F}_1$ is likely to be the physically more realistic case where it is taken to be proportional to the actual linear forcing f, rather than its fixed value $f_0 = \frac{1}{2}\mu a_1$ at the minimum of the neutral stability curve. Figure 5 shows four lower hysteresis boundaries, for (*a*)

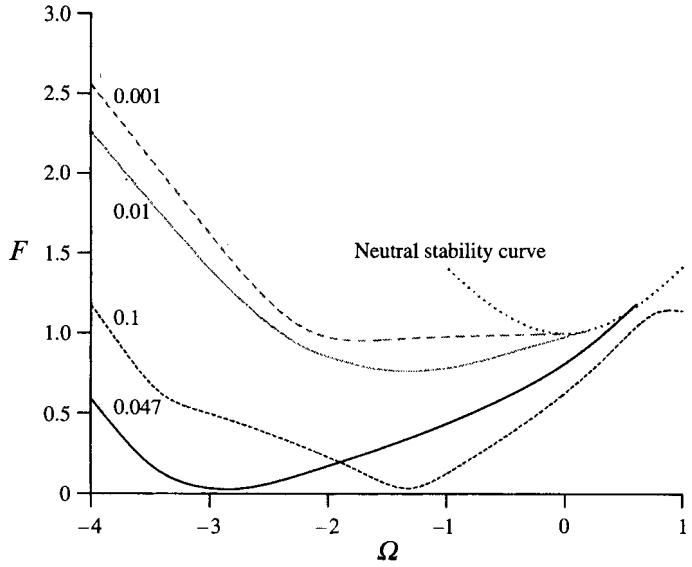

FIGURE 7. Existence of finite-amplitude fixed points for four different values of ϵ^2. Other parameters as in figure 5.

equation (5.1) with cubic forcing given by $\tilde{F}_1$, (*b*) equation (5.1) with cubic forcing given by $\tilde{F}_2$, (*c*) equation (1.3) with cubic forcing given by $\tilde{F}_1$ and (*d*) equation (1.3) with cubic forcing given by $\tilde{F}_1$ but with the coefficient of cubic damping chosen so that the boundary coincides with (*a*) vertically beneath the minimum of the neutral curve.

It can be seen that the effect of the fifth-order conservative term in (5.1) is to bend the lower hysteresis boundary and to shift the minimum in the lower hysteresis boundary to smaller values of the frequency Ω. Bending of the lower hysteresis boundary was seen also in §§4.1 and 4.3 and Appendix D, again caused by the fifth-order conservative term. Craik & Armitage (1995) pointed out that choosing the coefficient of cubic forcing to be $\tilde{F}_1$ rather than $\tilde{F}_2$ (see (5.4)) will cause the lower hysteresis boundary to bend. Comparing the three lower hysteresis boundaries in figure 5, it can be seen for this example that the presence of the fifth-order conservative term curves the lower hysteresis boundary far more than the effect produced by using $\tilde{F}_1$ instead of $\tilde{F}_2$.

The effect of varying the coefficient of cubic damping N is shown in figure 6 for a depth of 1.3 cm. These graphs show our model (5.1) along with $\tilde{F}_1$ (from (5.4)) for six different values of N. The line for $N = -5$ shows the type of diagram that Douady (1990) used to explain his observations, where hysteresis was not found, while the lines with $N > 0$ show hysteresis similar to that observed by Simonelli & Gollub (1989) and Craik & Armitage (1995).

Figure 7 shows the effect on the lower hysteresis boundary of varying ϵ^2. As expected, as ϵ^2 tends towards zero, the hysteresis boundary approaches the horizontal line $F = \mu$.

Figure 8 shows the experimental data plotted on the same diagram as the lower hysteresis boundaries predicted by our model (5.1) with $\tilde{F}_1$, for a variety of values of the coefficient of cubic damping N, where the other coefficients have been chosen to match the experimental situation at depth 1.3 cm. This allows a value of N to be selected which gives the best agreement between theory and experiment, and hopefully this gives a good estimate of the parameter. (Milner (1991) and Miles (1993) offer

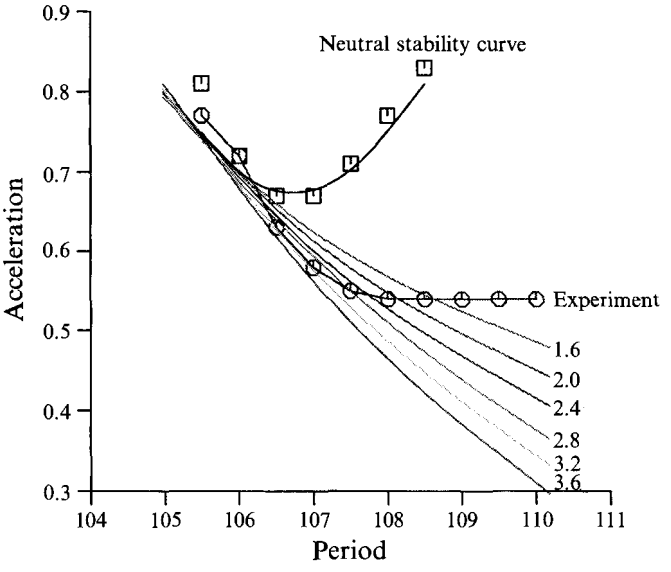

FIGURE 8. Lower hysteresis boundaries (calculated by considering the existence of fixed points) from our model (5.1) with $\tilde{F}_1$ for six different values of N, compared to equivalent experimental results.

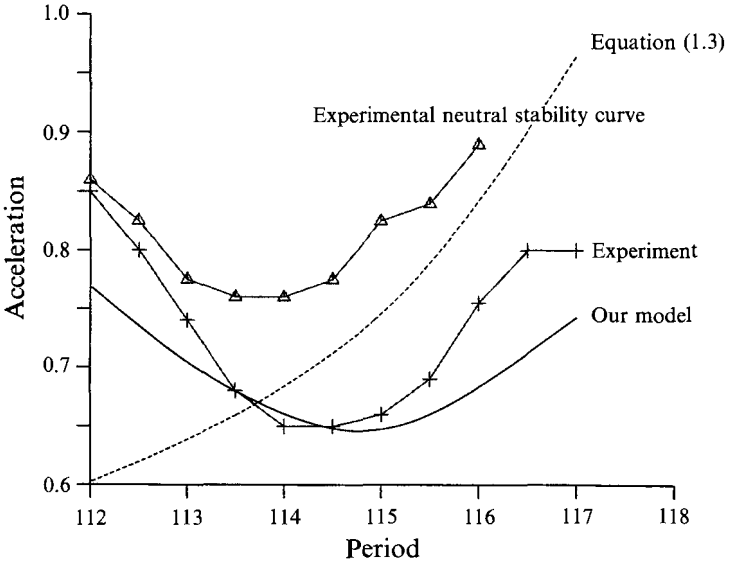

FIGURE 9. Comparison between theoretical and experimental lower hysteresis boundaries for a water depth of 1 cm, showing the boundaries predicted by our model (5.1) and by equation (1.3), as well as the experimental lower hysteresis boundary and neutral stability curve, for acceleration (m s^{-2}) against period (ms). Parameters are $N = -0.43$ (-0.68 for equation (1.3)), $\mu = 1$, $h = -0.85$, $\Pi = -0.82$, $\Gamma = 2.7$, $\epsilon^2 = 0.053$.

analytical expressions for N, but both rely upon assumptions that do not hold in our case.) However, it can be seen that there is not a unique theoretical curve which best agrees with the experimental results, and the choice is subjective.

The ultimate test of this paper is whether our model gives significantly better agreement with experimental results than the previously most accurate model. A comparison is

made, here and in §6, between our model (5.1) (with cubic forcing given by $\tilde{F}_1$) and with experimental results, for all three depths for which observations are available. The results are shown in figures 9 and 10. For both models, and for each depth, the coefficient of cubic damping N used in the computations was selected to give the 'best' agreement between that model and experimental results. The criterion used for this selection (except in figure 10(*c*) – see §6) was to choose the value of N which fixes the theoretical lower hysteresis boundary at the same point as the experimental boundary when $\Omega = 0$, i.e. vertically beneath the minimum of the neutral stability curve. Obviously other criteria could have been adopted.

Figure 9 shows the comparison between theory and experiment for the 1 cm depth case. The experimental results for figure 9 come from Craik & Armitage (1995) (22 half-wavelengths). Two things should be noted about the 1 cm depth case. First, the coefficient Π has changed sign from the 1.3 cm depth experiment, and this results in a qualitative difference. Secondly, the minimum observed in the lower hysteresis boundary (see figures 5, 6 and 7) has been shifted into frequencies Ω where it is observed physically.

Figures 10(*a*) and 10(*b*) show the comparisons for water depth of 1.3 cm and 2 cm (the 2 cm depth experimental results come from the 22 half-wavelength observations of Craik & Armitage 1995). The two graphs show the boundaries computed from (5.1) by considering the existence of stationary points. Figure 5 shows that for the 1.3 cm depth experiment, the lower hysteresis boundary calculated from (5.1) (line *a*) lies above the boundary calculated from (1.3) (line *d*), in the experimental frequency range. So we can see from figure 10(*a*) that (5.1) gives better agreement with the experiment than (1.3). The extra bending of the lower hysteresis boundary caused by the fifth-order conservative term is the main cause of this improvement. Similarly, the 2 cm depth observations are closer to the boundary given by (5.1) than the boundary given by (1.3).

Agreement between theory and experiment is satisfactory, but not spectacularly good. In particular, the trend of the experimental results at the greatest periods (for the two larger depths) is not well captured theoretically. The work of the next section suggests why this is so.

6. Stability of finite-amplitude solutions

Stability of the finite-amplitude wave solutions will now be considered. If A_0 is a stationary solution of (5.1), and $A = A_0 + B$ where B is small, then the combined evolution equation becomes, upon linearization with respect to B,

$$\begin{aligned}\dot{B} = &-\mu B + \mathrm{i}\Omega B + \mathrm{i}FB^* + \mathrm{i}\Pi |A_0|^2 B \\ &+ 2\mathrm{i}\Pi A_0 (\operatorname{Re} A_0 \operatorname{Re} B + \operatorname{Im} A_0 \operatorname{Im} B) + 3\mathrm{i}\epsilon^2 F\Gamma A_0^2 B \\ &+ \epsilon^2 N |A_0|^2 B + 2\epsilon^2 N A_0 (\operatorname{Re} A_0 \operatorname{Re} B + \operatorname{Im} A_0 \operatorname{Im} B) \\ &+ 3\mathrm{i}\epsilon^2 F\Gamma |A_0|^2 B^* + 6\mathrm{i}\epsilon^2 F\Gamma A_0^* (\operatorname{Re} A_0 \operatorname{Re} B + \operatorname{Im} A_0 \operatorname{Im} B) \\ &- \mathrm{i}\epsilon^2 h |A_0|^4 B - 4\mathrm{i}\epsilon^2 h A_0 |A_0|^2 (\operatorname{Re} A_0 \operatorname{Re} B + \operatorname{Im} A_0 \operatorname{Im} B). \end{aligned} \tag{6.1}$$

Expressing B in (6.1) in terms of real and imaginary parts as $B = B_r + \mathrm{i}B_i$ gives two real equations. These can be rewritten in the form

$$\begin{pmatrix} \dot{B}_r \\ \dot{B}_i \end{pmatrix} = M \begin{pmatrix} B_r \\ B_i \end{pmatrix}, \tag{6.2}$$

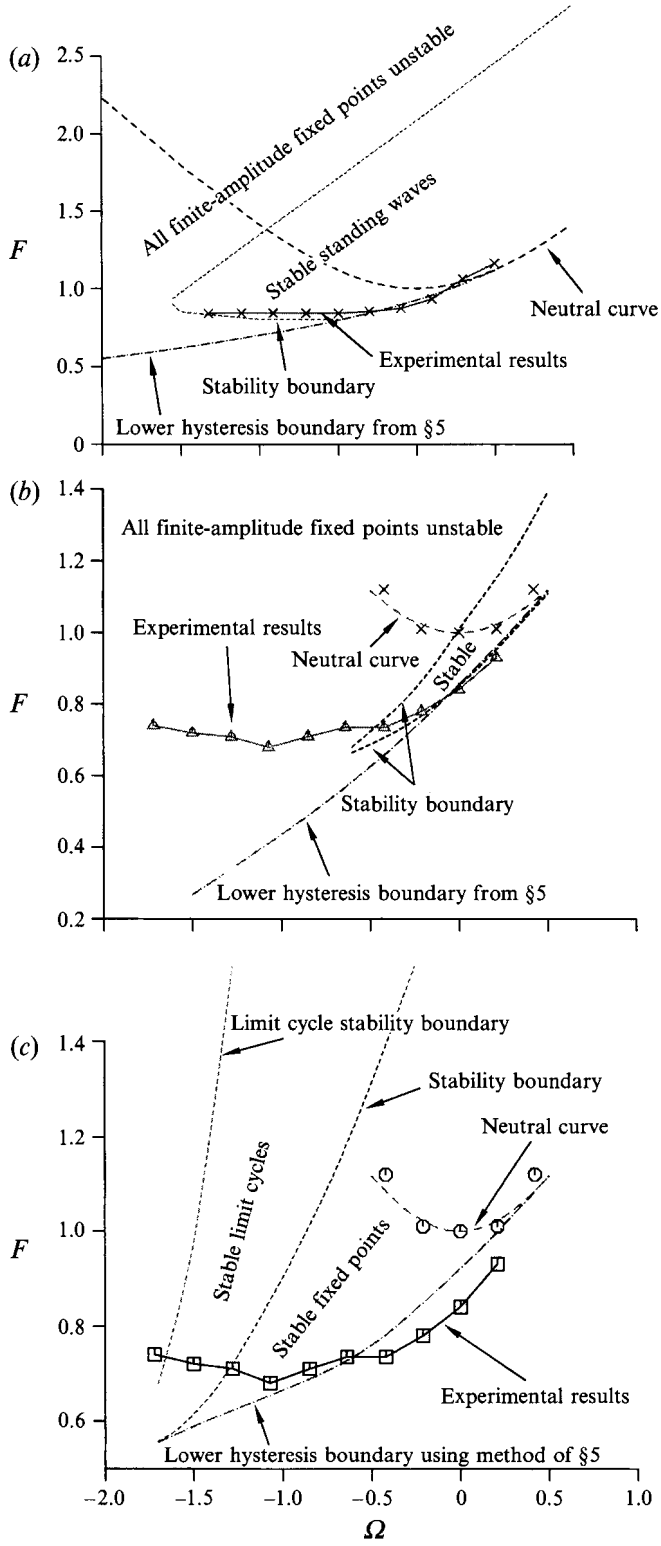

FIGURE 10. For caption see facing page.

where M is a two-dimensional real matrix. The characteristic equation of M is

$$\begin{aligned}
&\sigma^2 + 2\sigma\{\mu - 2\epsilon^2 N|A_0|^2\} \\
&\quad + \mu^2 + \Omega^2 - F^2 + 3(\epsilon^4 N^2 + \Pi^2 - 6\epsilon^4 \Gamma^2 F^2)|A_0|^4 \\
&\quad + 4(\Pi\Omega - \mu\epsilon^2 N - 3\epsilon^2 \Gamma F^2)|A_0|^2 + 2F|A_0|^2 \cos 2\phi (6\epsilon^2 \Omega\Gamma - \Pi) \\
&\quad - 2F\epsilon^2 N|A_0|^2 \sin 2\phi + 4\epsilon^2 F \cos 2\phi |A_0|^4 (h + 3\Pi\Gamma) \\
&\quad - 12\epsilon^4 F\Gamma h|A_0|^6 \cos 2\phi + 18\epsilon^4 F^2\Gamma^2|A_0|^4 \cos 4\phi \\
&\quad - 12\epsilon^4 NF\Gamma|A_0|^4 \sin 2\phi - 6\epsilon^2 \Omega h|A_0|^4 - 8\epsilon^2 \Pi h|A_0|^6 + 5\epsilon^4 h^2|A_0|^8 = 0, \qquad (6.3)
\end{aligned}$$

where σ is an eigenvalue so that B_r and B_i are both proportional to $\mathrm{Re}\, e^{\sigma t}$. This allows the stability of finite-amplitude solutions A_0 to be investigated, using the following algorithm.

For a given value of the forcing F and frequency Ω, all stationary solutions A_0 are found numerically (see §5). Each of these in turn is substituted into (6.3), resulting in a quadratic equation in σ, for each stationary point. The stability of each stationary point is determined by solving the corresponding quadratic equation and examining the real part of the eigenvalues. If any of the available stationary points is stable then the point (Ω, F) can be labelled as a stable point in parameter space. This is repeated over a fine grid of (Ω, F) points, giving a stability diagram in the forcing-frequency plane.

Figure 10(*a*) shows the results for the 1.3 cm depth experiment. Two regions are identified: one region indicates the existence of stable finite-amplitude stationary solutions (corresponding to self-stable standing waves); the other region describes where the finite-amplitude stationary solutions are all unstable. The dashed line gives the boundary between these two regions (this line is labelled the *stability boundary*). This line bifurcates from the lower hysteresis boundary calculated in §5 near to the point $\Omega = -0.5$, $F = 0.76$. Remarkably, the experimental lower hysteresis boundary almost coincides with this theoretical stability boundary. Accordingly, here there is very good agreement between theoretical and experimental results, when the stability of equilibrium points, as well as their existence, is taken into account.

For the 1 cm depth observations, all finite-amplitude stationary points were found to be stable. (This is because the estimated coefficient of cubic damping is negative in this case.) Therefore taking stability into consideration does not give an improved theoretical prediction for the lower hysteresis boundary calculated in §5, for this depth.

Figure 10(*b*) shows the stability diagram for the 2 cm depth experiment. Here the agreement is not so good, with the experimental points following the lower stability boundary, but continuing out of the stable region into the unstable region. However, if the coefficient of cubic damping (which as explained in the previous section was chosen in a rather *ad hoc* fashion) is chosen differently, then better overall agreement with the stability calculation can be achieved. Figure 10(*c*) shows the stability diagram for $N = 3.7$ (as opposed to $N = 6.4$ for figure 10*b*). Here the lower hysteresis boundary calculated in §5 coincides with the lower stationary point stability boundary. In this case, limit cycles were investigated as well as fixed points. This was done by numerically solving the evolution equation (5.1) with a Runge–Kutta scheme, for a variety of initial conditions. Figure 10(*c*) suggests that some of the standing waves observed in the

FIGURE 10. Stability diagrams for water depths of (*a*) 1.3 cm (*b*) 2 cm with $N = 6.4$ and (*c*) 2 cm with $N = 3.7$. Parameters are (*a*) $N = 2.43$, $\mu = 1$, $h = -2.1$, $\Pi = 0.25$, $\Gamma = 1.1$, $\epsilon^2 = 0.047$, (*b*) and (*c*) $\mu = 1$, $h = -2.1$, $\Pi = 0.42$, $\Gamma = 0.59$, $\epsilon^2 = 0.047$.

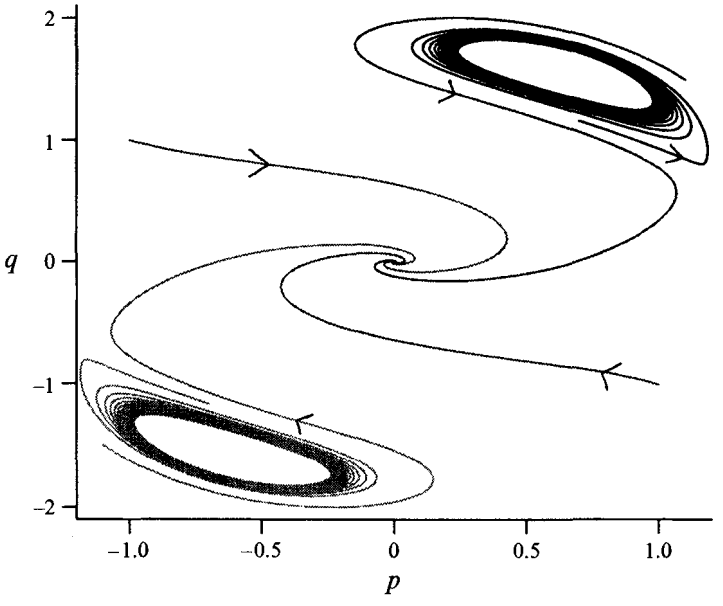

FIGURE 11. Phase plane diagram for figure 10(*c*) at $\Omega = -1.5$, $F = 0.7$.

experiment were stable limit cycles, rather than stable stationary points. An example of stable limit cycles is given in figure 11, which shows a phase plane diagram for $\Omega = -1.5$, $F = 0.7$. Physically a stable limit cycle corresponds to a standing wave where the amplitude experiences a slow oscillation on top of the fast sinusoidal oscillation of the wave motion. It can be seen that the limit cycles are relatively small compared with the amplitude $|A| = (p^2+q^2)^{1/2}$, so this small modulation would not be easily observed in an experiment. Further work is in progress on time-dependent solutions of (5.1).

7. Conclusions

We have examined, both theoretically and experimentally, the hysteresis region within which a flat surface or standing waves may occur, with Faraday excitation. We have confirmed the important roles of nonlinear cubic forcing and damping terms, previously incorporated into theoretical models by Miles (1993) and Craik & Armitage (1995); but we also find that a fifth-order conservative frequency shift must not be neglected.

The variational method due to Miles (1976) has been extended to allow the coefficient of this term to be calculated. This involved a significant use of symbolic computation. The Lagrangian given in §2 can be used in future to calculate the coefficient of the fifth-order conservative term for different geometries and for multiple wave interaction problems. We suggest that the fifth-order conservative term may also be important in other fields of interest in Faraday resonance, for example, pattern selection processes. Our derivation has also led to a correction of Miles' (1993) estimate of the coefficient of cubic forcing.

We have not calculated the damping coefficients theoretically. However, we show how the coefficients of linear and of cubic damping can be estimated from the experimental data: but the latter estimate remains a rather subjective one. For depths 1.3 cm and 2 cm, our estimates show the cubic damping coefficient to be positive, and

so opposite in sign to linear damping; but both damping coefficients appear to have the same sign for the 1 cm depth. (A purely theoretical determination of the cubic damping coefficient is a difficult task that we have not yet attempted: but see Milner 1991 and Miles 1993.)

The lower hysteresis boundary is normally the boundary above which any finite-amplitude stationary points exist, since locally-stable stationary points are then usually present. However, in some cases, these stationary points may all be unstable; then the lower hysteresis boundary should correspond to the boundary of stability of the stationary points. We have obtained local analytical results for the hysteresis boundary in §§4.1–4.3. Global numerical results for a composite evolution equation are given in §5 and questions of stability are treated in §6.

Good agreement between theory and experiment is achieved for our 1.3 cm water depth case, when fixed point stability is taken into account. Agreement with the 1 cm and 2 cm depth observations of Craik & Armitage (1994) is also quite good: but, for the latter, we conjecture that some observations may have corresponded to stable limit cycles, predicted by our model, rather than to stable stationary points.

S.P.D. thanks the Engineering and Physical Sciences Research Council for their support through an earmarked studentship.

Appendix A. Experiment

Experiments have been conducted using the same long rectangular tank as in Craik & Armitage (1995). Standing waves of 21, 22 and 23 half-wavelengths were examined in a Perspex tank of length 69.9 cm, width 2.82 cm and depth 7.7 cm which was suspended from two flat springs, allowing only vertical motion. The tank was driven by two vibrators, one near each end, connected in a series circuit. The circuit also contained a control box for the vibrators (setting frequency and acceleration of forcing), a counter to measure the frequency of oscillation and resistors to balance the two vibrators. A plate accelerometer was used to measure the r.m.s. forcing.

The depth of water used was 1.352 cm (measured using a vernier scale telescope). Fine controls on the legs of the base of the apparatus allowed the tank to be levelled. Distilled water was used with Kodak Photoflow wetting agent (proportion of wetting agent to water approximately 1:393) to reduce capillary hysteresis effects on the Perspex walls and to avoid problems with inadvertent contamination of the surface. To reduce evaporation, a lid was added. The accelerometer was used in conjunction with the resistors to balance the vibrators by measuring the acceleration of the tank at each end when no waves were present; the output of the accelerometer could also be examined on an oscilloscope to check that the motion of the tank was sinusoidal.

A frequency of oscillation would be chosen with an initial acceleration that was too small to generate waves on a flat surface. The forcing was then gradually increased with an increment of about 0.01 m s^{-2}, with this being maintained for at least ten minutes each time before making a further change. When the forcing crossed over the neutral stability boundary, then it took about ten minutes for the standing waves to slowly build up from the flat surface. As in Craik & Armitage (1995), frequencies were chosen so that three-dimensional waves that vary across the width of the tank were avoided. Once a standing wave was obtained, the forcing was slowly decreased again until the wave disappeared. This whole process was repeated for a range of frequencies.

Also a particular standing wave mode could be followed by slowly changing the frequency of oscillation. In this way, the lower hysteresis boundaries were found to

extend beneath the neutral stability curves of neighbouring wave modes. As the frequency was further altered, the standing wave would suddenly jump to another mode with one less half-wavelength.

Figure 1 shows the experimental results for 21, 22 and 23 half-wavelengths. These are similar to the experimental results of Craik & Armitage (1995) for their 2 cm depth case, but unlike the results of their 1 cm depth case.

Appendix B. An example of the derivation of (3.22)

The derivation of (3.22) is very algebraically demanding. It has been performed using the symbolic manipulation package MAPLE and the algebra covers several hundred pages. The average Lagrangian (3.4) has not been given fully in this text and the h coefficient in (3.22) has not been given except for two limiting cases. Here we will show the derivation in more detail by choosing a particular numerical example. The parameters chosen for this are $m = 23$ half wavelengths in a channel length of $l = 0.7$ m and depth $d = 0.01352$ m. The capillary length is taken to be $\lambda = 0.002$ m. Taking (2.30) and (3.14) gives the natural frequencies and the wavenumbers of the primary mode and its harmonics. These can be used to calculate (2.20) to (2.23). Substituting (3.1), (3.2) and (3.3) into (2.31), averaging over a $2\pi/\omega$ interval of t and using (3.5) gives

$$\begin{aligned}\langle L\rangle = {}&\text{Terms in } \epsilon^4 \text{ already given in (3.4)}\\
&+\epsilon^6 10^{-3}\Big\{0.614\left(\frac{\partial p}{\partial \tau_2}q-\frac{\partial q}{\partial \tau_2}p\right)+0.635(p^2+q^2)^3\\
&+0.307\left(\left(\frac{\partial p}{\partial \tau_1}\right)^2+\left(\frac{\partial q}{\partial \tau_1}\right)^2\right)-0.614F_1^2-0.137F_2^2-0.0712F_3^2\\
&+56.1f_1(p^2-q^2)+61.2f_0(p^4-q^4)+112f_0(pD_1+qE_1)\\
&+p(1.30D_1-0.189D_3)(p^2-3q^2)\\
&+q(1.30E_1-0.189E_3)(3p^2-q^2)\\
&+2.46(D_1^2+E_1^2)+0.176(D_2^2+E_2^2)+0.0353(D_3^2+E_3^2)\\
&+0.563(p^2+q^2)\left(\frac{\partial p}{\partial \tau_1}q-\frac{\partial q}{\partial \tau_1}p\right)\Big\}\\
&+O(\epsilon^8).\end{aligned} \tag{B 1}$$

This corresponds to (3.4) with (3.5) substituted into it.

Note that $\omega = \omega_1$ in (B 1) since it is not necessary to have the h coefficient dependent upon ω. We are interested only in stationary solutions here so put $\partial p/\partial \tau_1 = \partial q/\partial \tau_1 = 0$. The average Lagrangian can now be made stationary with respect to variations in D_n, E_n and F_n. When these expressions are substituted back into the Lagrangian it becomes

$$\begin{aligned}\langle L\rangle = {}&\text{terms in } \epsilon^4\\
&+\epsilon^6 10^{-3}\left\{0.614\left(\frac{\partial p}{\partial \tau_2}q-\frac{\partial q}{\partial \tau_2}p\right)+31.7f_0(p^4-q^4)\right.\\
&\left.-0.211(p^2+q^2)^3-0.0384\mu^2(p^2+q^2)+56.1\frac{f_1}{\epsilon^2}(p^2-q^2)\right\}\\
&+O(\epsilon^8).\end{aligned} \tag{B 2}$$

This gives the evolution equation (i.e. (3.22) and (3.23) without N-term)

$$\left.\begin{aligned}\frac{\partial p}{\partial \tau_2} &= 183 f_1 q + 206 f_0 q^3 - 2.07 q(p^2+q^2)^2 + 0.125\mu^2 q,\\ \frac{\partial q}{\partial \tau_2} &= 183 f_1 p + 206 f_0 p^3 + 2.07 p(p^2+q^2)^2 - 0.125\mu^2 p,\end{aligned}\right\} \tag{B 3}$$

which therefore gives $h = -2.07$ in this case. The last term in each equation in (B 3) is a small frequency shift term. This type of term has already appeared in (3.6) and it can be absorbed into $i\Omega A$ to cause a shift in the origin on the hysteresis diagram. (Since the coefficient is very small this shift will be negligible.) Note that the dependence upon the coefficient of linear damping comes from (3.8*b*) and (3.12).

Appendix C. Comparison with Miles (1993)

The cubic forcing coefficient calculated in Miles (1983) differs from the one calculated here (3.23) because Miles considered the first and second harmonics, but not the third harmonic. We find that there are two contributions to the cubic forcing: a cubic interaction between the first and second harmonics and the forcing (which Miles (1993) included), and a quadratic interaction between the third harmonic and the forcing (which Miles (1993) omitted). (However, it should be pointed out that the extra work in calculating the quadratic interaction between the third harmonic and the forcing is considerable, and if Miles had carried out this calculation then he would have been in a position to calculate the fifth-order conservative term as well if he had chosen.)

We can rewrite our expression in terms of depth, surface tension and wavenumber parameters, so as to enable comparison with Miles' (B 3) expression. In the limiting case of zero surface tension, we get for our expression

$$\tilde{F} = f k_1 \frac{(4\cosh^2(k_1 d)+3)(4\cosh^2(k_1 d)-1)}{16\tanh(k_1 d)(\cosh^2(k_1 d)-1)^2} \tag{C 1}$$

and for Miles' coefficient

$$\tilde{F}_{Miles} = f k_1 \frac{\tanh(k_1 d)(4\cosh^4(k_1 d)-1)}{4\cosh^2(k_1 d)(\cosh^2(k_1 d)-1)}. \tag{C 2}$$

For the limiting case of infinite depth, we get

$$\tilde{F} = f k_1 \frac{16g^3 + 9g^2 y k_1^2 + 6g y^2 k_1^4 + 40 y^3 k_1^6}{16(g+k_1^2 y)(g-2k_1^2 y)(g+4k_1^2 y)}, \tag{C 3}$$

while for Miles' coefficient

$$\tilde{F}_{Miles} = f k_1 \frac{(g+yk_1^2)^2}{(g+4yk_1^2)(g-2yk_1^2)}, \tag{C 4}$$

where $y = \gamma/\rho$.

Notice that as the depth tends towards infinity in (C 1) and (C 2), and as the surface tension tends towards zero in (C 3) and (C 4), then all four of the above expressions

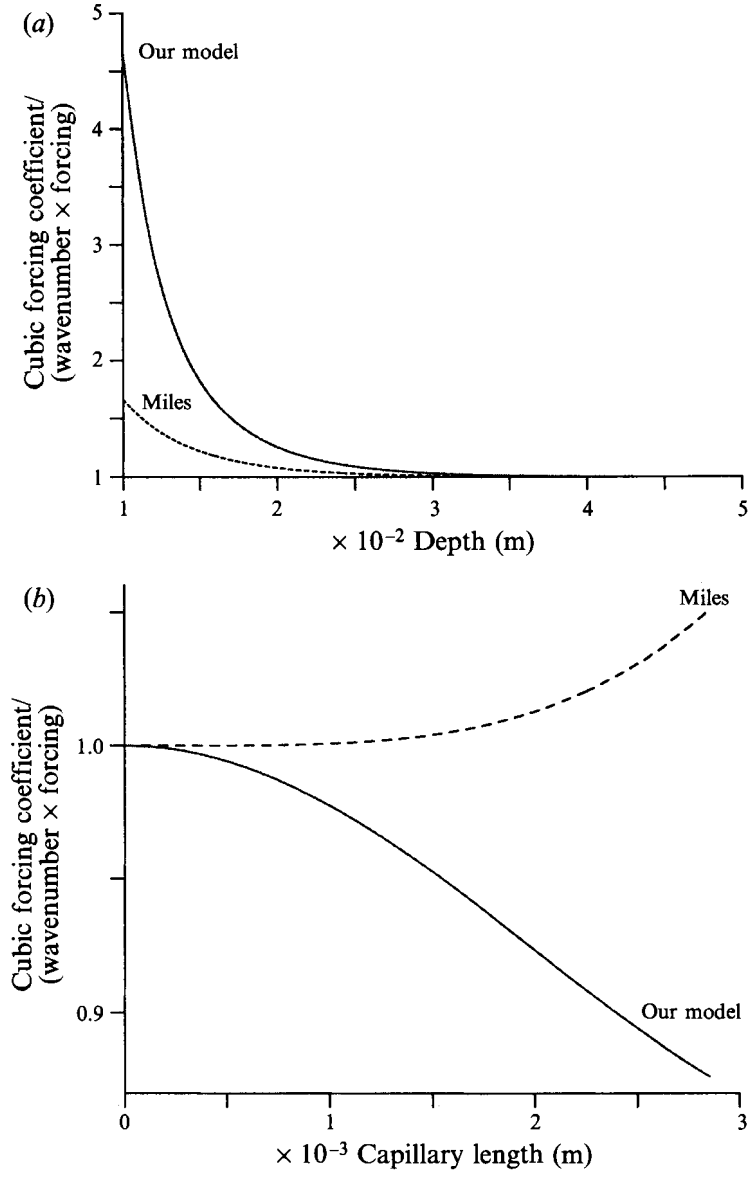

FIGURE 12. (*a*) Coefficient of cubic forcing given by (C 1) and (C 2). (*b*) Coefficient of cubic forcing given by (C 3) and (C 4).

tend towards fk_1. Figure 12 shows how our coefficient compares to Miles' coefficient over a range of depths and surface tensions.

Appendix D. The bending of the lower hysteresis boundary by the fifth-order conservative term

It has already been remarked in §5 that the fifth-order conservative term is found to bend the lower hysteresis boundary in computational studies of the evolution equation (5.1). Here the local analysis of §4.1, which gave an expansion for the lower hysteresis boundary (4.8), will be extended in order to demonstrate this effect analytically.

Evolution equations (3.6) and (3.22) have already been determined. If one is justified in neglecting the fifth-order damping and forcing terms as well as the seventh-order conservative term (which we do for simplicity), then the next evolution equation in this sequence is

$$\frac{\partial A}{\partial \tau_3} = \mathrm{i}\bar{F}_2 A^* + \mathrm{i}\tilde{F}_1(A^3 + 3|A|^2 A^*), \tag{D 1}$$

where $\bar{F}_2 = (2/a_1)f_2$ and $\tilde{F}_1 = f_1(\tilde{F}_0/f_0)$ are small corrections to the linear and cubic forcing coefficients respectively, with the forcing now expanded as

$$f = f_0 + \epsilon^2 f_1 + \epsilon^4 f_2 + O(\epsilon^6). \tag{D 2}$$

Note that a third slow time $\tau_3 \equiv \epsilon^6 \omega t$ has been introduced.

Now we perturb about (3.12) and (4.8). Equation (4.1) is extended to

$$p + \mathrm{i}q = u + \mathrm{i}v + \epsilon^2(r + \mathrm{i}s) + \epsilon^4(R + \mathrm{i}S) + O(\epsilon^6). \tag{D 3}$$

Again $C = u + \mathrm{i}v$, $B = r + \mathrm{i}s$ and $G = R + \mathrm{i}S$ giving (4.2) to (4.8). At the highest order the system of equations takes the form

$$\begin{pmatrix} \Omega - \mu & \Omega + \mu \\ -\Omega + \mu & -\Omega - \mu \end{pmatrix} \begin{pmatrix} R \\ S \end{pmatrix} = \begin{pmatrix} P \\ Q \end{pmatrix}, \tag{D 4}$$

where P and Q are known functions of (u, v, r, s).

From (4.5),

$$r = \frac{c - (\Omega + \mu)s}{\Omega - \mu} \quad (\Omega \neq \mu). \tag{D 5}$$

Putting (4.7) into (4.6) gives

$$c = -d = \pm \frac{h\Omega^2}{2\Pi^2}\left(\frac{-2\Omega}{\Pi}\right)^{1/2}. \tag{D 6}$$

For (D 4) to be consistent, we require that $P + Q = 0$. This is, however, a single equation in two unknowns, namely $\bar{F}_2$ and s, if (D 5) and (D 6) are substituted into $P + Q = 0$. We require to find $\bar{F}_2$, but clearly we cannot do so while s remains unknown.

Now we can write

$$r + \mathrm{i}s = b_1 \exp(-\tfrac{1}{4}\mathrm{i}\pi) + b_2 \exp(\tfrac{1}{4}\mathrm{i}\pi). \tag{D 7}$$

The second component of (D 7) lies along $u + \mathrm{i}v$ since phase $(u + \mathrm{i}v) = \frac{1}{4}\pi$. Therefore b_2 contributes only to an infinitesimal change in $|C| = (-\Omega/\Pi)^{1/2}$ and so an infinitesimal change in Ω. So, we may choose to set $b_2 = 0$, effectively without loss, to obtain

$$-r = s = \frac{c}{2\mu} = \pm \frac{h\Omega^2}{4\mu\Pi^2}\left(\frac{-2\Omega}{\Pi}\right)^{1/2}. \tag{D 8}$$

Then, phase $(r + \mathrm{i}s) = -\frac{1}{4}\pi$, the component b_1 being orthogonal to $u + \mathrm{i}v$.

The calculation which gives (4.9) is readily completed, using

$$\tilde{F}_1 = \frac{\tilde{F}_0 \Omega}{\mu\Pi}(N + 2\tilde{F}_0) \tag{D 9}$$

which comes from (3.8), (3.12) and (4.8).

REFERENCES

BENJAMIN, T. B. & URSELL, F. 1954 The stability of the plane free surface of a liquid in vertical periodic motion. *Proc. R. Soc. Lond.* A **225**, 505–517.

CRAIK, A. D. D. 1994 The stability of some three-dimensional and time-dependent flows. *IUTAM Symp. Potsdam, NY: Nonlinear Instability of Nonparallel Flows* (ed. S. P. Lin, W. R. C. Phillips & D. T. Valentine), pp. 382–396. Springer.

CRAIK, A. D. D. & ARMITAGE, J. 1995 Faraday excitation, hysteresis and wave instability in a narrow rectangular wave tank. *Fluid Dyn. Res.* **15**, 129–143.

DOUADY, S. 1990 Experimental study of the Faraday instability. *J. Fluid Mech.* **221**, 383–409.

FARADAY, M. 1831 On the forms and states of fluids on vibrating elastic surfaces. *Phil. Trans. R. Soc. Lond.* **52**, 319–340.

MILES, J. W. 1967 Surface-wave damping in closed basins. *Proc. R. Soc. Lond.* A **297**, 459–475.

MILES, J. W. 1976 Nonlinear surface waves in closed basins. *J. Fluid Mech.* **75**, 419–448.

MILES, J. W. 1984 Nonlinear Faraday resonance. *J. Fluid Mech.* **146**, 285–302.

MILES, J. W. 1993 On Faraday waves. *J. Fluid Mech.* **248**, 671–683.

MILES, J. W. & HENDERSON, D. 1990 Parametrically forced surface waves. *Ann. Rev. Fluid Mech.* **22**, 143–165.

MILNER, S. T. 1991 Square patterns and secondary instabilities in driven capillary waves. *J. Fluid Mech.* **225**, 81–100.

NAGATA, M. 1989 Nonlinear Faraday resonance in a box with a square base. *J. Fluid Mech.* **209**, 265–284.

SIMONELLI, F. & GOLLUB, J. P. 1989 Surface wave mode interactions: effects of symmetry and degeneracy. *J. Fluid Mech.* **199**, 471–494.

UMEKI, M. 1991 Faraday resonance in rectangular geometry. *J. Fluid Mech.* **227**, 161–192.

UMEKI, M. & KAMBE, T. 1989 Nonlinear dynamics and chaos in parametrically excited surface waves. *J. Phys. Soc. Japan* **58** (1), 140–154.